This manuscript is a preprint and has been formally accepted for publication in **Basin Research**.

What Controls Salt-Detached Contraction in the Translational Domain of the Outer Kwanza Basin, Offshore Angola?

Aurio Erdi[1,2], Christopher A-L. Jackson[1]

[1]Basin Research Group (BRG), Department of Earth Science and Engineering, Imperial College, London, SW7 2BP, United Kingdom
[2]Research Center for Geotechnology, Indonesian Institute of Science, Indonesia

Correspondence

Aurio Erdi, Basin Research Group (BRG), Department of Earth Science and Engineering, Imperial College, Prince Consort Road, London, SW7 2BP, United Kingdom.

Email: a.erdi18@imperial.ac.uk

Funding Statements/Information

Indonesia Education Scholarship (BPI), Indonesia Endowment Fund for Education (LPDP), Grant/Award Number: 201712220212151

Data Availability Statement

The seismic data supporting the findings of this study are available from CGG. However, restrictions apply to the availability of these data, which were used under license for this study.

ORCID ID

Aurio Erdi

https://orcid.org/0000-0003-4247-715X

Christopher A-L. Jackson

https://orcid.org/0000-0002-8592-9032

Abstract

It is now well-established that base-salt relief drives complex deformation patterns in the mid-slope domain of salt-bearing passive margins, in a location classically thought to be dominated by simple horizontal translation. However, due to a lack of detailed studies drawing on high-quality, 3D seismic reflection data, our understanding of how base-salt relief controls four-dimensional patterns of salt-related deformation in natural systems remains poor. We here use 3D seismic reflection data from, and structural restorations of the Outer Kwanza Basin, offshore Angola to examine the controls on the evolution of variably oriented salt anticlines, rollers, and walls, and related normal and reverse faults. We show that the complex geometries and kinematics of predominantly contractional salt structures reflect up to 22 km of seaward flow of salt and its overburden across prominent base-salt relief. More specifically, this contractional deformation occurs where the seaward flow of salt is inhibited due to: (a) it flowing being forced to flow up, landward-dipping ramps; (b) it encountering thicker, slower-moving salt near the base of seaward-dipping ramps; or (c) the formation of primary salt welds at the upper hinge of seaward-dipping ramps. The rate at which salt and its overburden translates seaward varies along strike due to corresponding variations in the magnitude of base-salt relief and, at a larger, more regional scale, primary salt thickness. As a result of these along-strike changes in translation rate, overburden rotation accompanies bulk contraction. Our study improves our understanding of salt-related deformation on passive margins, highlighting the key role of base-salt relief, and showing contraction, extension and rotation are fundamental processes controlling the structural style of the mid-slope translational domains of salt basins.

Keywords: passive margin, section restoration, salt weld, salt tectonics, shortening, base-salt relief, structural geology

1. Introduction

Salt-bearing passive margins are typically characterised by thin-skinned, gravity-driven deformation above a salt layer. Kinematically-linked domains of the deformation form (e.g. Brun and Fort, 2004, 2011; Rowan et al., 2004), with the upslope domain represented by extensional structures such as salt-detached faults and associated salt rollers and rafts (e.g. Duval et al., 1992; Lundin 1992; Rowan et al., 1999; Brun and Mauduit, 2009), whereas the downslope domain is represented by contractional structures such as salt anticlines and salt-detached thrusts (e.g.

Cramez and Jackson, 2000; Hudec and Jackson, 2004). These two domains are commonly connected by an intermediary, mid-slope, translational domain (e.g. Cramez and Jackson, 2000; Davison et al. 2012; Quirk et al., 2012; Jackson et al., 2015), which has historically been viewed as an area of relatively little deformation, characterised primarily by horizontal translation. However, relatively recent studies using 2D seismic reflection data (or 2D profiles through 3D data) and physical models have demonstrated that the mid-slope domain can be strongly deformed, and can experience multiple phases of extensional and contractional deformation, if the salt and its overburden translate seaward above base-salt relief and/or encounter salt weld (Fig. 1a, c) (e.g. Dooley and Hudec, 2017; Ferrer et al., 2017; Dooley et al., 2017; 2018; Duffy et al., 2019). Ramp-syncline basins (RSBs) may also develop within this domain if base-salt relief is present (e.g. Jackson and Hudec, 2005; Peel, 2014; Pichel et al., 2018; Evans and Jackson, 2019). Despite offering an improved understanding of the regional kinematics of salt-bearing passive margins, regional studies using only 2D seismic data are limited in that they provide only a two- rather than three-dimensional view of how base-salt relief controls mid-slope salt tectonics and related overburden deformation. Furthermore, we have a poor understanding of how salt welding, a key process during salt tectonics, impacts horizontal translation and related salt-related structural style. Ultimately, studies of natural systems help to test the predictions of physical models (e.g. Brun and Fort, 2004; 2011).

A recent study by Evans and Jackson (2019) used 3D seismic reflection data from the mid-slope domain of the Outer Kwanza Basin, offshore Angola to show how base-salt relief controlled the temporal and spatial development of ramp-syncline basins (RSBs) (Fig 2a). Their three-dimensional study of this natural salt-tectonic system also showed how changes in the downdip volumetric flux and velocity of the salt caused local extension or contraction of the salt and its overburden, associated with local acceleration or deceleration of the salt, respectively. This interaction with base-salt relief created locally variable strain fields that deformed the salt and its overburden, overprinting the broader, margin-scale salt tectonics typically associated with gravity gliding and spreading. Evans and Jackson (2019) also suggest that an along-strike (to the SE) increase in regional salt thickness resulted in the salt and its overburden translating seaward. As a result, ramp-syncline basins and associated salt diapirs were rotated clockwise during translation. Their study, however, did not establish how the specific base-salt structural configurations in the mid-slope domain controlled specific salt-related structural styles, nor spatial variations in the rate of seaward translation of the salt and its overburden.

Our study develops the ideas presented in and uses the kinematic framework defined by Evans and Jackson (2019) to show that the mid-slope translational domain can be strongly deformed in response to multiphase extension and contraction. As predicted by physical models, this complex deformation relates to the translation of salt and its overburden above base-salt relief. Our high-quality 3D seismic reflection dataset allows us to examine the spatial distribution of and relationship between base-salt relief, salt thickness and salt structural style, and the supra-salt structural framework. By restoring several sub-regional seismic profiles, we identify the impact these relationships have on the location and rate of seaward translation of salt and its overburden. Furthermore, we demonstrate that base-salt relief and the formation of primary salt welds are key controls on the geometry, distribution, and kinematics of contractional structures in the mid-slope domain of salt basins (Fig 1a, c).

2. Geological Setting

The Outer Kwanza Basin is an offshore sub-basin of the Kwanza Basin, Angola (Fig. 2) (Lundin, 1992; Brownfield and Charpentier, 2006; Jackson and Hudec, 2009). The basin is separated from the Inner Kwanza Basin by a basement high called the Flamingo Platform, and it is bound at its western end by the Angola Abyssal Plain and at its southern end by several volcanic seamounts. To the north, the Outer Kwanza Basin passes into the Lower Congo Basin (Hudec and Jackson, 2002; 2004; Jackson and Hudec, 2005; Brownfield and Charpentier, 2006).

The Kwanza Basin initially formed during the Early Cretaceous rifting associated with the opening of the South Atlantic Ocean (Fig. 3). Rifting is recorded by the development of N-to-NW-trending ridges, a NE-trending transform margin, and the formation of numerous horst-and-graben systems in the present offshore area (Karner and Driscoll, 1999; Hudec and Jackson, 2002, 2004; Brownfield and Charpentier, 2006; Guiraud et al., 2010; Serié et al., 2017). During the latter stages of rifting, in response to the onset of more restricted marine conditions, a thick (up to 1.4 km), Aptian salt-dominated unit was deposited, draping residual rift-related basement highs and regional thickening westward (i.e. seawards) and southward (i.e. along-strike) (Marton, 2000; von Nicolai, 2011; Evans and Jackson, 2019). The salt is presently relatively thick in the Outer Kwanza Basin, gradually thinning eastward onto the Flamingo Platform, where it is locally absent (Hudec and Jackson, 2002; 2004; Karner et al., 2003; Jackson and Hudec, 2005).

Aptian salt controlled post-rift, gravity-driven deformation and the overall tectono-stratigraphic evolution of post-Aptian sequences in the Outer Kwanza Basin (Duval et al., 1992; Lundin, 1992;

Marton et al., 2000; Quirk et al., 2012). This gravity-driven salt-tectonic system comprises kinematically-linked zones of updip extension above the Flamingo Platform and downdip contraction towards the seaward edge of the salt (Fig. 2) (Hudec and Jackson, 2002; 2004). The intervening zone of bulk translation is defined by a range of structural styles that appear to define three main phases of deformation (Fig. 3) (Evans and Jackson, 2019). First, during the Albian, local contractional and extensional deformation occurred due to seaward salt flow across a series of base-salt ramps, resulting in the formation of salt anticlines and rollers. Second, during the Cenomanian to Oligocene, regional seaward tilting of the margin occurred, driven by post-rift thermal subsidence focused along the western edge of the Outer Kwanza Basin. This initiated regional seaward gliding, translation, and rotation of the overburden above base-salt relief. During this phase, salt flow across base-salt highs generated overburden extension and the formation of rafts, and locally, where contraction occurred, salt anticlines. Third, during the Oligocene and Miocene, salt-detached seaward translation and rotation of the overburden continued. Local extension drove reactive diapirism and the rise of salt walls, in some cases by the breaching of the roofs of previously formed salt anticlines. Elsewhere, in contractional strain fields, some pre-existing structures were locally shortened. Finally, uplift of the African continent during the Miocene to Recent continued to drive seaward translation of salt and rotation of the overburden, but at an accelerated rate. Translation, and local shortening and rotation caused squeezing and active rise of some salt walls. Salt welding, and an increase in sediment accumulation rate relative to diapir rise rate, eventually led to the burial of salt structures and a decrease in margin-scale salt tectonics.

We focus on an area located between the seaward-edge of the Flamingo Platform, just south of the Martin Vaz Transform Fault and above several rift-related horsts (Fig. 2; i.e. in the ‘diapir’ and ‘monocline’ domains of Hudec and Jackson, 2004; see also Guiraud et al., 2010). The diapir domain contains a range of salt structures formed in response to extension and contraction (i.e. salt anticlines, rollers, walls, and sheets) (Hudec and Jackson, 2004; Evans and Jackson, 2019). The monocline domain contains RSBs formed due to the seaward translation of salt and its overburden (e.g. Jackson and Hudec, 2005; Dooley et al., 2017; 2018; Pichel et al., 2018; 2019; Evans and Jackson, 2019). By analysing these RSBs and flanking salt structures, Evans and Jackson (2019) showed that overburden in this area underwent total of c. 23 km of seaward translation and a clockwise plan-view rotation of c. 32º. However, we here demonstrate that magnitude of the seaward translation and rotation might not represent regional-scale kinematics related to large-scale, along-strike changes in salt thickness; instead, this style of deformation may reflect the more local control of base-salt relief.

3. Dataset and Methods

3.1 Datasets and seismic interpretation

This study uses 1276 km^2 of a 2,915 km^2, zero-phase processed, post-stack depth migrated (PSDM) BroadSeis^{TM} 3D seismic dataset that covers the Outer Kwanza Basin, offshore Angola (Fig. 2). Due to confidentiality reasons, the data are cropped at the base-salt (c. -5.5 km). However, the morphology of the base-salt surface, which controls many of the salt-related structural styles documented here and by Evans and Jackson (2019), is clear. This dataset has inline (northwest-southeast) and crossline (northeast-southwest) spacing of 25 m; inlines and crosslines are oriented broadly normal and perpendicular to the bulk south-westerly translation direction, respectively. The seismic dataset has a record length of 10 km and a vertical sample rate of 2 m, with a vertical resolution of c. 3.5 m and c. 30 m at the seabed and at a depth of c. 5 km, respectively. The data are displayed with the Society of Exploration Geophysicists (SEG) 'normal' polarity convention; i.e. a downward increase and decrease in acoustic impedance are represented by a positive reflection (white) and a negative (black) reflection event, respectively. We mapped eight seismic horizons, the ages of which are determined by comparing our data to age-constrained regional seismic profiles presented by other authors (see Table 1). Age constraints allow us to establish the relative timing of different salt-tectonic events by identifying key seismic-stratigraphic relationships (e.g. onlap, truncation).

3.2 Restoration analysis

Quantitative structural restorations were undertaken on several SW-trending cross-sections oriented broadly parallel to the regional (salt) tectonic transport direction. These restorations allowed us to: (a) validate our seismic interpretation; (b) unravel the two-dimensional evolution of salt-related local contractional structures; (c) illustrate the quasi-3D kinematics of salt-related deformation using serial 2D cross-sections; and (d) calculate spatial variations in the magnitude of seaward translation of the suprasalt (see Appendix A for full detail information of restoration, methodology, and algorithms). A key constraint on our structural restoration were the RSBs, which are inferred to initiate at the top of fixed (i.e. static) base-salt ramps (cf. Hudec and Jackson, 2004;

Jackson and Hudec, 2005; Rowan and Ratliff, 2012; Dooley and Hudec, 2017; Dooley et al. 2017; 2018).

4. Base-salt Structural Style

We first describe the morphology of the base-salt; this provides a spatial framework for understanding the base-salt-induced deformation identified within the salt and its overburden (Fig. 4a). The base-salt dips broadly to the SW. Superimposed on this are three distinctive trends (i.e. NW-, N-, NE-trending) defined by relatively steeply dipping ramps (>10°). In the northeast, the ramps trend NW, are *c.* 36-km long, and dip up to 47° seaward, defining the seaward edge of the Flamingo Platform (Figs 2, and 6-7). In the southwest and the south, the base-salt ramps trend NW-to-N and dip up to 25 °, forming an array of concave, seaward-dipping ramps (Figs 4a, 5a, b, c and 6b). Between the north-eastern, and southern and south-eastern areas, we identify four structural highs that define local relief of *c*. 500-1000 m. These four highs trend NW-to-N and are bound by dip of 10-45° dipping ramps that face either landward or seaward (V, W, X, Y and Z; Figs 4a, 5a, 6a, b and 7). Although our lack of sub-salt seismic imaging means we cannot identify the origin of these structural highs and flanking ramps, the dips of the ramps are consistent with the dips of subsalt normal faults (~50°) identified in the Lower Congo Basin (cf. Zone 2 of Moulin et al, 2005); thus, we speculated the local highs and associated ramps are fault-bounded and may be related to the Angola-Gabon horst-block system (*sensu* Hudec and Jackson, 2004). The relatively flat relief (<10°) such as in the southwest and southeast (Figs 5a, 6b, and 7b, c), however, may reflect pre-rift growth strata without significant extensional faulting (cf. Zone 3 of Moulin et al, 2005). In the north and the southeast, we observe relatively short (<11 km long), NE-trending ramps that face either SE or NW, and which locally intersect a NW-trending ramp (Fig. 4a). These NE-trending ramps are consistent with the trend of the Martin Vaz Transfer Fault (Fig. 2a) (*sensu* Moulin et al., 2005; Guiraud et al., 2010); we thus infer these ramps are the upper crustal expression of this lithosphere-scale structure.

5. Distribution and Style of Salt and Supra-salt Structures

The geometry of salt and supra-salt structures varies across the study area. A salt-thickness map allows us to define the distribution of salt structures that are related purely to contraction (e.g. salt anticlines), and other structures of more variable origin (e.g. salt walls) (Table 2; Figs 4b and 5-7). Some salt structures are separated by primary welds, either apparent or incomplete (*sensu* Wagner and Jackson, 2011), across which supra-salt strata appear to directly overlie sub-salt strata (Fig. 7). A structure map of the Albian seismic horizon, which records the cumulative translation of the overburden, defines the *present* spatial relationships between salt and spatially related supra-salt structures (e.g. salt-detached normal faults, outer-arc bending-related normal faults, and thrusts and strike-slip faults; Table 3; Figs 4c and 5-7). As indicated by Evans and Jackson (2019), it is critical to note that: (a) the salt and supra-salt structures are unlikely to be in the same position as where they formed, given they have translated seaward a few tens of kilometres; and because of this (b) salt and supra-salt structures likely do not directly overlie the base-salt features that triggered their initial development. Finally, the salt and related supra-salt faults are overlaid by and occur within RSBs that formed purely in response to Eocene-to-Pliocene, salt-detached translation of the overburden (Figs 6 and 7b, c). However, as shown by Pichel et al. (2018), RSBs can be internally deformed by post-formation diapirism and salt-related faulting (above SN1; Fig. 6c).

Interpretative sketch maps of the main salt structures (as defined at the top salt structural level), the supra-salt structures (as defined at the Albian structural level), and a simplified base-salt structure map, show the *present* spatial relationship between features at all three levels (Fig. 8). Both the salt and supra-salt structures vary in terms of their distribution and orientation relative to underlying base-salt features (Table 2). For example, where they are elongate (e.g. anticlines, walls), they may lie either parallel or oblique to the ramps. In other cases, these features overlie relatively flat areas at base-salt (SA1 and SW2; Fig 5b). We now describe the geometry and interpret the origin and evolution of salt and salt-related structures, with a specific focus on salt-related contractional structures. The evolution of these structures is shown by the structural restoration of selected cross-sections (Fig. 9; see also Appendix C for a larger version of the restorations).

6. Salt-related Contractional Structural Style

6.1 Salt anticlines

6.1.1 Geometry

In the southwest, salt anticlines trend broadly parallel to NE-trending, base-salt ramps, or are presently located above relatively flat areas of the base-salt surface (SA in Table 2 and SA1; Fig. 8). The anticlines above the flat areas are polyharmonic, increasing in wavelength, but decreasing in amplitude, upwards (SA1; Figs 5b and 7b, c). These salt anticlines are commonly overlaid by relatively thick (up to 800 m) roofs, suggesting they formed in response to contraction (Jackson and Hudec, 2017). In the north, where the ramp changes to trend NW, the anticlines similarly change trend to stay sub-parallel to the underlying structures, being located above either seaward- or landward-dipping ramps (SA3-6; Fig. 8). Above seaward-dipping ramps, the limbs of these salt anticlines are commonly dissected by salt-detached normal faults, such as above the landward limb of SA4 (Fig. 6a), suggesting this anticline may have been later extended. From this point northeastward, these salt anticlines are overlain by thick roofs, underlain by still-thick salt, and have their seaward limbs offset by NW-SE-striking thrusts faults immediately above the downdip end of the underlying ramps (SA5 and SA6; Fig. 6a). In a few cases in the north of the study area, highly-deformed anticlines are presently located above seaward-dipping ramps (SN in Table 2 and SN1; Fig. 8a). These anticlines are characterised by a triangular salt pedestal, an apparent secondary weld (*sensu* Wagner and Jackson, 2011), and are sometimes overlain by normal faults inferred to accommodate outer-arc bending and stretching of the arched roof (SN1; Fig. 6c). Because of its associated with this range of features, we interpret that these types of salt anticlines were amplified and laterally squeezed in response to continued horizontal shortening.

6.1.2 Timing and Structural Evolution

The salt-cored anticlines, at least those in the southwest of the study area, initiated relatively early, in the Albian, given they are flanked and overlain by intra-Albian growth strata (SA1; Figs 5b, c, 6b, 7b and c). The salt anticlines may have formed due to: (a) buckling at the base of base-salt ramps, as relatively fast-moving thin salt encountered relatively slow-moving thicker salt (Jackson and Hudec, 2005; Evans and Jackson, 2019) (position labelled label 3; Fig. 1c); and/or (b) salt thickening, and overburden deceleration and shortening upon encountering landward-dipping base-salt ramps (i.e. in cases where the anticlines are presently located on base-salt plateaus; Fig. 1a) (cf. Dooley et al., 2017; 2018; Pichel et al., 2019). The former interpretation is, however, not consistent with several physical models, which predict that, during the early stages of translation, a monocline rather than a salt anticline may form at the top of a seaward-dipping base-salt ramp (Gaullier et al., 1993; Dooley and Hudec; 2017; Dooley et al., 2017; 2018). Although it is possible that such a monocline did form and was subsequently translated further seaward before growing into a salt anticline (Jackson and Hudec, 2005), we prefer the latter interpretation, given we consistently see thickened salt immediately seaward of landward-dipping ramps (SA5 and SA6; Fig. 6a).

Our structural restorations, which are based on the assumption that anticlines form due to translation across the landward-dipping side of base-salt highs, suggest salt anticlines in the southwest of the study area, initiated in the Late Albian (cf. Fig. 1a) (ii; Fig. 9a, b). We propose that the polyharmonic geometry of the salt anticlines, such as observed in the southwest, reflect continuous (rather than punctuated) local contraction during overburden thickening, followed by further seaward translation (cf. Fig. 1b) (SA1; Figs 5b, c, 7b, c and ii; Fig. 9a).

During the Eocene to Oligocene, new salt anticlines initiated and Early Cretaceous anticlines were amplified, as indicated by their flanking Eocene-to-Oligocene growth strata (SA4-6; Fig. 6a). This indicates that base-salt relief-related shortening of the overburden was diachronous across the study area, with salt anticlines starting to grow in the SW during Eocene, becoming younger and more deformed towards the NE (cf. SA4-6; Fig. 6a and SA3; Figs 6b).

Our structural restoration in the north of the study area reconstructs the Late Cretaceous-Paleogene location of the salt anticlines, suggesting that their diachronous growth was again associated with salt flow and overburden translation over local base-salt highs (ii-iv; Fig. 9c). More specifically, we see three key phases of anticline growth: (a) initiation due to the seaward flow of salt and its overburden over landward-dipping ramps in the Late Cretaceous-Early Eocene (ii; Fig. 9c) (cf. Fig. 2a); (b) local extensional faulting of the anticlines in the Late Eocene as they translated across the seaward-dipping ramps (iii; Fig. 9c) (cf. position labelled 2; Fig. 1c); and (c) further seaward translation of the anticlines, and formation of seaward-verging thrusts as the salt and its overburden passed over landward-dipping ramps during the Oligocene (iv, Fig. 9c).

During the Miocene to Holocene, some pre-existing salt anticlines were locally influenced by contraction. For example, in the southwest, Middle Miocene strata onlap onto underlying strata and are dissected by outer-arc bending-related normal faults above salt anticlines, showing that, during Miocene-Holocene translation, salt anticlines were laterally squeezed (SN1; Figs 5d and 6c and Table 2). We suspect that this squeezing may reflect the contraction of the salt anticlines at the base of the seaward-dipping ramps as they passed through the contractional hinge (cf. position labelled 3 in Fig. 1b).

6.2 Salt walls

6.2.1 Geometry

Salt walls broadly trend either parallel or oblique to NW-to-N-trending ramps, being presently located above either the relatively flat parts of the base-salt or on landward-dipping ramps (SW and SS in Table 2, and SW1-3 and SS1; Fig. 8a). There are three types of salt wall. The first type have a broadly symmetrical, triangular profile, a well-defined, pointed crest, and are flanked by inward-dipping, salt-detached normal faults, geometries characteristic of their formation in response to reactive diapirism initiated by overburden extension (SW1; Fig. 5a) (e.g. Vendeville and Jackson, 1992a). In contrast to these morphologically and genetically simple reactive diapirs, we observe two additional types of rather more complex salt walls in the centre and northeast of the study area (SS1 and SW2; Figs 6c and 7).

The second type is represented by walls that vary in terms of their map-view trend and overall geometry, and which have variable spatial relationships with base-salt ramps (SW2; Fig. 8a). In the centre and the south of the study area, SW2 trends parallel to and is presently located downdip of NW-trending, seaward-dipping ramps, or relatively flat areas immediately seaward of these ramps (SW2; Fig. 7 b, c). Similar to the simple triangular salt walls described above, SW2 has a triangular profile and is flanked by inward-dipping, salt-detached normal faults. However, near its centre, SW2 has a rounded rather than pointed crest, whereas in the south, where the crest is pointed, the flanking faults have relatively shallow dips (<50º). Based on these geometrical characteristics, we infer that these walls initially formed as reactive diapirs, with their latter growth occurring in response to horizontal shortening (e.g. Vendeville and Jackson, 1992b). This shortening drove roof arching, rounding-off of the diapir crest, and the passive rotation of normal faults to lower dips. The northern end of SW2 presently trends parallel to and is located above-to-slightly downdip of, a seaward-dipping ramp (SW2; Fig. 7a). Here, SW2 is capped by an irregular, indented crest, which is associated with a salt horn (SW2; Fig. 5d). By comparison to geometries formed in physical models, we infer that this distinctive structural style formed in response to extension-driven diapir fall. This fall was possibly related to the flow of salt along strike within the wall to feed another part of the structure that was actively rising in response to synchronous shortening (e.g. Vendeville and Jackson, 1992a).

The third type of salt wall is represented by structures trending parallel to, and presently located above or slightly downdip of NW-trending, seaward-dipping ramps, or the relatively flat areas immediately seaward of these ramps (SS1-3; Fig. 8a). At its northern end, SS1 is presently located above a relatively flat part of the base-salt. In this location, SS1 is flanked by inward-dipping faults overlying a triangular salt pedestal, an incomplete secondary weld (*sensu* Wagner and Jackson, 2011), and an arched roof (Fig. 6c), features characteristic of a reactive diapiric wall that was subsequently squeezed (see Vendeville and Nilsen, 1993; Rowan et al., 2004; Jackson et al., 2008; Dooley et al., 2009). We observe another two walls of this complex type in the northeast of the study area; these structures, which are separated by a primary weld and which overlie a NW-trending, seaward-dipping ramp, are both geometrically similar to SS1, but are both characterised by thrusted roofs (Table 3 and SS2-3; Fig. 7a). Here, at the base of this ramp, SS2 is characterised by a very well-defined triangular profile, is flanked by inward-dipping faults, and a NW-SE-striking, landward-dipping thrust above its crest (SS2; Fig. 7a). However, further to the northwest, SS2 appears to be overlain by outer-arc extensional faults, being located above a rollover monocline (see Fig. 6b and Table 3). Thrusts, similar to those observed further to the southeast, are lacking. Based on these characteristics we suggest that the monocline formed due to draping of overburden across the western flank of the SS2, which originally formed as a reactive diapir. This folding induced the formation of outer-arc bending-related normal faults in the roof of SS2; the structure and its overburden were subsequently shortened, and related faults reactivated to form the crestal fore-thrust.

6.2.2 Timing and Structural Evolution

The age of growth strata indicate that salt walls began to grow in the Eocene to Oligocene. For example, Late Cretaceous-to-Eocene strata locally onlap onto underlying (Albian) strata and fill RSBs (Fig. 7b, c) or thicken across reactive diapir-flanking faults (SW1; Fig. 5a and SW2; Fig. 7a). Oligocene growth strata are also locally contained in RSBs. Locally, however, Late Cretaceous-to-Oligocene strata are tabular adjacent to and upturned against diapir flanks, suggesting these structures are younger and that reactive diapir growth was diachronous (SS2, SS3; Fig. 7a and SW2; Fig. 7b, c).

The structural restorations show that in the north and the south of the study area, Albian salt anticlines had by the Eocene-Oligocene, translated seaward onto either the flat-topped structural highs or seaward-dipping ramps, resulting in crestal extension and the formation of reactive salt walls (SW2 and SS2-3 in iii-iv; Fig. 9a, b). Based on our restorations, we propose two mechanisms that may have caused local overburden extension and reactive diapir rise. First, an increase in the velocity of the seaward flow above the local structural high resulted in the widening of a pre-existing salt anticline, and the formation of extensional faults in its overburden (location labelled 1; Fig. 1c) (see late-stage buildup of thick salt body above high block of Jackson and Hudec, 2017; see also Dooley et al., 2017; 2018). Second, the seaward flux of salt was retarded as salt flowed across the upper hinge of the seaward-dipping ramp, resulting in overburden extension (location labelled 2; Fig. 1c) (see extensional hinge of Jackson and Hudec, 2017; see also Dooley et al., 2017; 2018). Our key interpretation is that seaward-translating, pre-existing anticlines underwent subsequent extension to become reactive diapirs in the Late Cretaceous-Oligocene. Local contraction did occur in the Oligocene, as evidenced by local arching and thinning of

Oligocene strata over walls like SS1 (Fig. 6c). We suggest this contraction was driven by translation of the walls towards the lower hinge of the seaward-dipping ramps, where they encountered relatively thick, slower-moving salt (location labelled 3; Fig. 1c) (see contractional hinge of Jackson and Hudec, 2017; see also Dooley et al., 2017; 2018).

By the Miocene, salt and its overburden had translated a significant distance seaward (11-21 km; Fig. 10); this is comparable to the distance calculated by Evans and Jackson (2019) (i.e. 18 km) based on their study of ramp-syncline basins in the SE of the study area. This translation is recorded in the formation of RSBs and resulted in the continuous growth and/or local contraction of pre-existing diapirs as they passed over base-salt relief (Figs 6 and 7).

During the Early-Middle Miocene, SS2 and SS3 continued to grow, before they are shortened and squeezed at the end of the Middle Miocene. Continued reactive growth of these walls is indicated by presence of an upturned collar of Early-Middle Miocene growth strata that thicken across flanking, salt-detached normal faults (SS2-3; Fig. 7a). Subsequent shortening is recorded by the erosional truncation of Middle Miocene strata across the diapir crest.

The structural restoration shows that, during the Early-Middle Miocene, pre-existing (reactive) salt walls continued to grow (SS2-3 in v; Fig. 9b). We speculate that the continued growth of these walls was influenced by local extensions above the seaward-dipping ramps (c.f. location labelled 2; Fig. 1c). Furthermore, at the end of the Middle Miocene, whereas some salt walls continued to grow, SS2 continued translating seaward before undergoing contraction at the base of a seaward-dipping ramp, reverse reactivating the former salt-detached normal fault responsible for its initial growth, and resulting in the formation of a fore-thrust (vi; Fig. 9b) (c.f. location labelled 3; Fig. 1c).

During the Late Miocene, SS2 and SS3 continued shortening. This shortening is recorded by thinning of Upper Miocene strata across the thrust-bound block capping the diapirs (SS2-3; Fig. 7a). Our structural restoration suggest that a primary weld formed above a local structural high at this time, with SS2 and SS3 were being squeezed at the base and top, respectively, of the underlying seaward-dipping base-salt ramp (vii; Fig. 9b). At the base of the ramp, squeezing caused rotation and welding of the eastern flank of the SS2, whereas further updip this caused reverse reactivation of a salt-detached normal fault above SS3, such that it now resembles a back-thrust. Three possible mechanisms might account for generating local contraction and this change in structural style during the Late Miocene. The first is retardation of the seaward flow of salt as it encounters local base-salt highs; this could have caused salt thickening, overburden shortening, and fault inversion (see Ferrer et al., 2017). However, this interpretation is considered unlikely because, from this point northwestward, salt-detached normal faults rather than thrusts are presently observed above many salt structures (Figs 6b and 8b). As such, the local base-salt high does not appear to have driven the repeated inversion of normal faults to form back-thrust as the salt structures translated seaward above seaward-dipping ramps. The second mechanism might reflect slowing of salt and shortening of its overburden as they travel onto a seaward-dipping ramp (c.f. location labelled 3; Fig. 1c). Although this mechanism may reasonably explain the generation of the fore-thrust, it is considered unlikely as a sole mechanism because local contraction above seaward-dipping ramps has not been documented in physical models; i.e. salt flow onto a seaward-dipping ramp induces contraction rather than extension (location labelled 2; Fig. 1c) (Jackson and Hudec, 2017; Dooley et al., 2017; 2018).

Given the spatial relationship between base-salt structures, salt walls, and supra-salt faults during the Late Miocene, inferred from our structural restorations, we suggest shortening and thrusting were driven by a combination of the salt slowing, overburden shortening and primary welding above the seaward-dipping ramp (vii; Fig. 9b). We interpret that whereas the growth of the fore-thrust (i.e. above the SS2) was associated with local contraction at the base of the ramp, the updip weld act as a buttress that inhibited further seaward flow of salt, resulting in overburden shortening and inversion of the former salt-detached normal fault (i.e. above the SS3). Our interpretation is consistent with the predictions of physical models, which indicate that salt pinch-out above seaward-dipping ramps can induce overburden shortening and thrusting (c.f. Dooley, et al., 2007).

During the Miocene, SW2 was subjected to active rise in the south of the study area and extension-driven fall in the centre. In the south, active rise initiated in the Early Miocene; this is indicated by the onlap of Early Miocene strata onto Oligocene strata adjacent to SW2 (Fig. 7b, c). Active rise continued during the Middle-Late Miocene, as reflected by overall thinning of upturned Middle-Late Miocene strata against the diapir flank. In the central part of the study area, however, extension-driven fall initiated in the Middle Miocene, as indicated by the Middle Miocene strata draping over a relic horn at the crest of the northern margin of SW2 (Fig. 5d). Extension-driven fall continued into the Late Miocene, as indicated by thickening of Late Miocene strata across normal faults in the diapir roof (SW2; Figs 5d and 7a).

Our structural restorations across the central and southern parts of the study area highlight the Miocene development of SW2. In the south, SW2 underwent active rise as it entered a contractional strain field at the base of a seaward-dipping ramp (v-vii; Fig. 9a). In contrast, at its centre, SW2 underwent initially extension-driven reactive rise as the diapir travelled onto a seaward-dipping ramp and went through the extensional hinge, and then extension-driven fall (v-vii; Fig. 9b). We suggest that diapir fall was associated with the along-strike flow of salt from the northern part of SW2 in the centre to feed actively rising portions of the wall in the south (see also Vendeville and Jackson, 1992b).

By the Pliocene-Recent, some walls were inactive and completely buried, whereas others continued to grow via shortening-induced active diapirism or extension-driven reactive diapirism. Synchronous shortening and extension is well-illustrated in the centre of the study area, where Pliocene-to-Recent growth strata thin onto an inversion-related fold above SS3, whilst similar-age strata thicken across the salt-detached normal faults on the eastern flank of the SW2 (Fig. 7a). In the south, however, Pliocene-to-Recent strata are folded and eroded above SW2, with Late Miocene strata presently exposed at the seabed (Fig. 7b). This observation indicates that locally at least, SW2 continues to actively rise. This is likely driven by ongoing translation, an interpretation consistent with the observation that Pliocene-to-Recent strata fill still-active RSBs (Fig. 7b) (see also Evans & Jackson, 2019).

7. Translation Magnitude and the Tectonic Evolution of the Mid-Slope Domain, Outer Kwanza Basin

We here link our detailed analysis of the geometry and evolution of salt-related structures and sub-regional structural restorations with the RSB-determined, rotation magnitude estimates of Evans and Jackson (2019) (Fig. 10) to generate seven sequential maps illustrating the three-dimensional, salt-tectonic evolution of the mid-slope domain of this segment of the Outer Kwanza Basin, offshore Angola (Fig. 11). These maps show the initial (i.e. Early Albian) location of salt and supra-salt structures relative to base-salt features, and their subsequent evolution as they translated seaward. For ease of description, these maps are grouped into three main salt-tectonics phases (i.e. Early Cretaceous, Late Cretaceous-Paleogene, and Neogene-Present).

7.1 Early Cretaceous

The Early Cretaceous was characterised by base-salt relief-induced folding of the overburden in the south and centre due to spatial and temporal variations in the magnitude and thus rate of seaward translation; i.e. the magnitude was c. 3.7 and 10.5 km in the centre and south, respectively (Figs 10 and 11a). In contrast and as indicated by the presence of tabular Albian strata, the northern domain did not translate or undergo significant salt tectonics at this time (i; Figs 9c and 10). The cause of this along-strike variability is not obvious, but it might reflect the fact that Aptian salt was thicker (von Nicolai, 2011) and, therefore, possibly faster flowing in the south (Evans and Jackson, 2019). Regardless of the cause, we speculate that this variability led to the salt and its overburden being mildly sheared and/or undergoing bulk, rigid-body, clockwise rotation (Fig. 11a).

7.2 Late Cretaceous-Paleogene

The Late Cretaceous-Paleogene was dominated by reactive diapirism and salt wall formation, with this being particularly common in the centre and the northeast due to increasing salt flow velocity above either local structural highs (i.e. flat-topped) or the outer-edge of the Flamingo Platform (i.e. seaward-dipping ramps) (Fig. 11 b, c). Local shortening in the north initiated the growth of salt anticlines above the landward-dipping ramps, and in the southwest, where the precursor anticlines amplified as they rotated across concave-into-the basin, seaward-dipping ramps. Anticline rotation due to along-strike variations in seaward salt flux meant that these structures presently have a wide range of trends (cf. convergent gliding pattern of Cobbold and Szatmari, 1991). Anticline tightening initiated the growth of outer-arc bending-related normal faults in their roofs.

Synchronous extension-driven diapirism and contraction-driven salt-detached folding reflect spatial differences in the rate of seaward translation of the salt and its overburden. More specifically, during the Oligocene, the total magnitude of the translation in the north, where translation did not occur until the Eocene, surpassed that in the centre, where translation started earlier (i.e. Late Albian) (Fig. 10). In the north, along-strike variations in the magnitude of translation were accommodated by the local growth of strike-slip faults that are particularly well-developed in the north (Fig. 5a, d and Table 3). In the south, the variation in the translation magnitude resulted in more distributed strain in the form of seemingly bulk overburden rotation in the SE (i.e. 23°; Evans and Jackson, 2019) (Fig. 11c). Overburden rotation occurred because the seaward flow of salt slowed across local structural highs in the centre of the study area, whilst salt was able to flow faster in the southeast, an area of relatively subdued relief (Fig. 12) (cf. convergence of salt flow across isolated structural highs; Dooley et al., 2018).

7.3 Neogene-Present

Along strike variation in translation magnitude, as well as synchronous extension and contraction driven by salt flow across base-salt relief, continued into the Neogene. Variations in translation magnitude are clearly shown in the Miocene, when the translation rate was relatively stable in the north but accelerated in the centre and south (Fig. 10). These variations likely reflect along-strike changes in salt thickness, and the interaction between the salt, its overburden, and underlying base-salt relief. In the southwest, outer-arc bending-related normal faults formed at the crest of salt anticlines due to shortening and tightening of the precursor anticlines (SA1; Fig. 5b and Fig. 11 d, e, f). This shortening can be attributed to the relatively late, upslope migration of contraction that continues to the present (Brun and Fort, 2004; Fort et al., 2004). However, where anticlines were located above relatively flat areas of the base-of-salt immediately seaward of concave-into-the-basin, seaward-dipping ramps, we propose that anticline shortening was driven by convergent gliding (c.f. Cobbold and Szatmari, 1991). From this point northward and northeastward, squeezing and active rise of pre-existing walls and anticlines occurred, either at the base or top of seaward-dipping ramps (Fig. 11 d, e, f). At the same time, local extension induced reactive piercement of the overburden, resulting in the formation of rollers and rafts above the ramp defining the seaward-edge of the Flamingo Platform (vi; Figs 9a and 11e). These local, short length-scale variations between contractional and extensional structures reflect disparities in the magnitude and rate of seaward translation of the salt and its overburden, with this again being accommodated in the north by strike-slip faulting, and in the east by the bulk rotation of the salt and its overburden. Salt tectonics is presently modest in the mid-slope domain, and most salt and supra-salt structures are buried and inactive. Locally, however, active diapiric rise and deformation of the seabed attest to ongoing shortening (Fig. 11g).

Our structural restorations suggest that the total absolute translation magnitude varied along-strike of this segment of this salt-based passive margin (i.e. 13, 11, and 22 km in the north, centre, and south, respectively; Fig. 10). These values are generally less than those calculated by Evans and Jackson (2019) based on their analysis of RSBs and flanking salt walls located SE of the present study area (i.e. 23 km). We suggest two interpretations might plausibly account for the differences in these magnitude values: (a) salt was originally thicker(~1.3 km) in the SE, meaning the salt and its overburden flowed seaward relatively quickly compared to the NW (von Nicolai, 2011; Evans and Jackson, 2019); (b) the relief at base-salt varied along strike, being large in the north and centre where the translation magnitude was relatively small, and more subdued in the south where the magnitude was relatively large; in this interpretation, regional variations in salt thickness are less important (Figs 4a and 5a) (see Dooley et al., 2017; Dooley and Hudec, 2017).

8. Discussion

Classic models of salt-bearing passive margins state that salt-related deformation above relatively smooth base-salt relief are related to the kinematically-linked domains of updip extension, mid-slope translation, and downdip contraction (e.g. Marton et al., 2000; Hudec and Jackson, 2004; Rowan et al., 2014; Brun and Fort, 2004; 2011). This model cannot, however, explain the wide range of local patterns and styles of predominantly contraction-related salt structures seen on the mid-slope of the Outer Kwanza Basin, offshore Angola. Here, the mid-slope domain is characterized by the synchronous formation of extensional and contractional salt-related structures. Evans and Jackson (2019) invoked spatially complex salt flow over base-salt relief to explain this spatially complex pattern of deformation southeast of the present study area, illustrating the formation, translation, and rotation of RSBs and flanking salt walls. They highlight the key role played by the seaward-edge of the Flamingo Platform but they did not focus on the types and kinematics of contraction-related salt-tectonic structures. We show that local base-salt relief, and not only the Flamingo Platform, control the diversity and evolution of salt-related contractional styles in the mid-slope domain of the Outer Kwanza Basin. Similar relationships are documented in the Santos and Campos Basins, offshore Brazil, and in the Gulf of Mexico (e.g. Dooley et al., 2017; Dooley and Hudec, 2017; Pichel et al., 2019).

Several physical models explore the relationship between base-salt relief and salt tectonics, suggesting that salt flow across rugose relief, coupled with the formation of salt welds, can influence structural style. For example, Cobbold and Szatmari (1991) illustrate that salt flow across convex- and concave-towards-the-basin base-salt relief can generate arcuate arrays of extensional or contractional structures, respectively. More recently, Dooley et al. (2017; 2018) illustrate that salt flow and overburden across landward- and/or seaward-dipping ramps at base-salt can generate coeval contractional and extensional structures in areas otherwise dominated by simple horizontal translation (Fig. 1a, c). These models also show that deformation patterns can become especially complex where the base-salt relief is discontinuous along-strike (Fig. 12a). These local discontinues act to locally perturb salt flow, resulting in salt flow channelization (i.e. convergent and/or divergent) that can cause the salt and its overburden to rotate as the translate (Fig. 12b). Other physical models by Dooley et al (2007) show that salt may locally weld at the base of salt-detached thrusts during bulk shortening, resulting in increasing frictional drag along the salt-overburden interface. As shown by Duffy et al. (2019), salt welds such as this may causes otherwise freely horizontally translating minibasins to collide, inducing the formation of contractional structures.

Our study seismic reflection-based study of the mid-slope domain of the Outer Kwanza Basin allow us to test the predications of several physical models. Our observations, combined with our structural restorations, illustrate that the interaction between predominantly horizontally flowing salt and underlying base-salt relief resulted in complex strains. More specifically, contraction structures developed in the midst of an array of extensional structures, with mainly structures undergoing a multiphase history comprising both periods of extension and compression. For example, the translation of salt and its overburden across broadly margin-parallel ramps (i.e. NW and N-trending) causes not only early contraction and the formation of salt anticlines when salt was capped by a relatively thin roof, but also late extension and shortening of precursor salt structures (i.e. squeezing reactive and active rise of diapirs) as they are translated over multiple ramps (cf. Cobbold and Szatmari, 1991; Dooley et al., 2017; 2018).

Our study shows that the formation of mid-slope contractional structures is made even more complex due to the combined effect of bulk rotation (i.e. a type of distributed shear) of the salt overburden and pre-existing salt structures. Previous studies using 3D seismic reflection data suggest this rotation may be caused by salt flow across complex base-salt relief (i.e. isolated base-salt highs and/or convex- and concave-into-the-basin ramps) (Pichel et al., 2019), and/or spatial variations in the original salt thickness (Evans and Jackson, 2019). The results of our study are consistent with the latter hypothesis, but we also suggest that a key control on salt structure and overburden rotation is the presence of local base-salt relief (i.e. rotation only occurred in the south of the study area, where base-salt relief was more subdued). The broadly complex ramps and isolated base-salt highs in the north and centre of the study area perturbed seaward flow of salt and its overburden (cf. Fig 12; Dooley et al., 2018), resulting in salt flowing faster in the south. Concave-ramps in the southwest also served to amplify and rotate contractional structures as they translated seaward (cf. convergent gliding; Cobbold and Szatmari, 1991).

Primary and secondary salt welds formed in the mid-slope domain of the Outer Kwanza Basin during horizontal translation (cf. Dooley et al, 2007). The primary welds formed above seaward-dipping ramps, driving local squeezing of pre-existing extensional diapirs (walls) located on their updip, landward side. The process described here is similar to that described from the Northern Gulf of Mexico, where primary welding causes otherwise freely horizontally translating minibasins to collide, inducing the formation of contractional structures (see Duffy et al., 2019). In our study, weld-induced compression results in the reverse reactivation of previously extensional structures (i.e. normal faults) that initially formed near the upper hinge of seaward-dipping ramps (position labelled 2; Fig. 1c).

We argue that using the geometry and evolution of RSBs alone to understand the kinematics of salt-detached deformation yields an incomplete picture (e.g. Pichel et al., 2018; Evans and Jackson, 2019); such analyses should be supported by the detailed mapping of base-salt relief and overlying salt-tectonic structures. For example, rather than simply being associated with bulk clockwise rotation of the overburden (Evans and Jackson, 2019), we observe that RSBs are locally associated with the local growth of salt-detached strike-slip faults (i.e. a type of focused shear), at least in the northern part of the basin during the Late Miocene to Present (Fig. 11 f, g). The formation of strike-slip faults records spatial differences in the rate and magnitude of the seaward translation of salt and its overburden, with this effect maybe being either enhanced or retarded by the presence of base-salt relief. Where such relief is present, along-strike variations in translation may be relatively sharp, leading to focused shear and strike-slip faulting. Further work is required to establish the detailed geometric and kinematic relationship between salt-detached strike-slip faults and base-salt relief.

9. Conclusion

We used 3D seismic reflection data to examine the structural style, distribution, and kinematics of salt structures in the mid-slope domain of the Outer Kwanza Basin, offshore Angola. We showed that a suite of predominantly contractional salt-related structures, including salt anticlines and squeezed walls, as well as salt-detached thrusts, are observed in the midst of an array of extensional structures. These salt-related structures trend either parallel or oblique to, and are sometimes located directly above, NW-, N-, NE-trending ramps along the base-salt. Some of the structures are separated by either apparent or incomplete primary salt welds.

Using section restorations to identify the pre-translation location of the salt and salt-related structures, we argue that base-salt relief and the formation of primary salt welds controlled the presence and evolution of contractional salt-related structures. We also show that the seaward translation of salt and its overburden began in the Albian, soon after salt deposition, and that the absolute magnitude of translation varied from 13 to 22 km. The interaction between base-salt highs and salt welds, and the seaward-translating salt structures lead to locally intense overprinting of extensional and compressional strain fields. Seaward translation was also associated with bulk clockwise rotation of salt structures and related overburden structures. We suggest that during early translation, this rotation was driven by regional, along-strike changes in salt thickness, with thicker, faster-flowing salt and overburden in the SE and thinner, slower-moving salt and overburden in the NW. However, during later translation, as salt had locally thinned due to the flow of salt into growing diapirs, base-salt relief became relatively more important; i.e. in the north and centre, where base-salt relief was more pronounced, the seaward translation of salt and its overburden translation was more tortuous and overall slower compared to the south.

Our study can help improve our understanding of the styles and origin of salt-related deformation that can occur in salt basins. More specifically, our study further highlights the key role base-salt relief, salt thickness variations, and salt welding can play in driving surprisingly complex deformation in the mid-slope domain of salt basins. These learning can be applied to other salt basins and especially salt-detached passive margins.

Data Availability Statement

The seismic data supporting the findings of this study are available from CGG. However, restrictions apply to the availability of these data, which were used under license for this study.

References

Brownfield, M. E., and Charpentier, R. R., 2006, Geology and Total Petroleum Systems of the West-Central Coastal Province (7203), West Africa: U.S. Geological Survey Bulletin 2207-B, p. 52.

Brun, J.-P., and Fort, X., 2004, Compressional salt tectonics (Angolan margin): Tectonophysics, v. 382, no. 3-4, p. 129-150.

Brun, J.-P., and Fort, X., 2011, Salt tectonics at passive margins: Geology versus models: Marine and Petroleum Geology, v. 28, no. 6, p. 1123-1145.

Brun, J.-P., and Mauduit, T. P. O., 2009, Salt rollers: Structure and kinematics from analogue modelling: Marine and Petroleum Geology, v. 26, no. 2, p. 249-258.

Cobbold, P. R., and Szatmari, P., 1991, Radial gravitational gliding on passive margins: Tectonophysics, v. 188, no. 3-4, p. 249-289.

Cramez, C., and Jackson, M. P. A., 2000, Superposed deformation straddling the continental-oceanic transition in deep-water Angola: Marine and Petroleum Geology, v. 17, no. 10, p. 1095-1109.

Davison, I., Anderson, L., and Nuttall, P., 2012, Salt deposition, loading and gravity drainage in the Campos and Santos salt basins: Geological Society, London, Special Publications, v. 363, no. 1, p. 159-174.

Dooley, T. P., and Hudec, M. R., 2017, The effects of base-salt relief on salt flow and suprasalt deformation patterns — Part 2: Application to the eastern Gulf of Mexico: Interpretation, v. 5, no. 1, p. SD25-SD38.

Dooley, T. P., Hudec, M. R., Carruthers, D., Jackson, M. P. A., and Luo, G., 2017, The effects of base-salt relief on salt flow and suprasalt deformation patterns — Part 1: Flow across simple steps in the base of salt: Interpretation, v. 5, no. 1, p. SD1-SD23.

Dooley, T. P., Hudec, M. R., Pichel, L. M., and Jackson, M. P. A., 2018, The impact of base-salt relief on salt flow and suprasalt deformation patterns at the autochthonous, paraautochthonous and allochthonous level: insights from physical models: Geological Society, London, Special Publications, v. 476, p. SP476.413.

Dooley, T. P., Jackson, M. P. A., and Hudec, M. R., 2007, Initiation and growth of salt-based thrust belts on passive margins: results from physical models: Basin Research, v. 19, no. 1, p. 165-177.

Dooley, T. P., Jackson, M. P. A., and Hudec, M. R., 2009, Inflation and deflation of deeply buried salt stocks during lateral shortening: Journal of Structural Geology, v. 31, no. 6, p. 582-600.

Duffy, O. B., Fernandez, N., Peel, F. J., Hudec, M. R., Dooley, T. P., and Jackson, C. A. L., 2019, Obstructed minibasins on a salt-detached slope: An example from above the Sigsbee canopy, northern Gulf of Mexico: Basin Research, v. 32, no. 3, p. 505-524.

Duval, B., Cramez, C., and Jackson, M. P. A., 1992, Raft tectonics in the Kwanza Basin, Angola: Marine and Petroleum Geology, v. 9, no. 4, p. 389-404.

Evans, S. L., and Jackson, C. A. L., 2019, Base-salt relief controls salt-related deformation in the Outer Kwanza Basin, offshore Angola: Basin Research, v. 32, no. 4, p. 668-687.

Ferrer, O., Gratacós, O., Roca, E., and Muñoz, J. A., 2017, Modeling the interaction between presalt seamounts and gravitational failure in salt-bearing passive margins: The Messinian case in the northwestern Mediterranean Basin: Interpretation, v. 5, no. 1, p. SD99-SD117.

Fort, X., Brun, J.-P., and Chauvel, F., 2004, Salt tectonics on the Angolan margin, synsedimentary deformation processes: AAPG Bulletin, v. 88, no. 11, p. 1523-1544.

Gaullier, V., Brun, J. P., Gue´rin, G., and Lecanu, H., 1993, Raft tectonics: the effects of residual topography below a salt de´collement: Tectonophysics, v. 228, no. 3-4, p. 363-381.

GEBCO Compilation Group, 2020, The GEBCO_2020 Grid - a continuous terrain model of the global oceans and land, British Oceanographic Data Centre, National Oceanography Centre, NERC, UK (available at https://www.bodc.ac.uk/).

Guiraud, M., Buta-Neto, A., and Quesne, D., 2010, Segmentation and differential post-rift uplift at the Angola margin as recorded by the transform-rifted Benguela and oblique-to-orthogonal-rifted Kwanza basins: Marine and Petroleum Geology, v. 27, no. 5, p. 1040-1068.

Hudec, M. R., and Jackson, M. P. A., 2002, Structural segmentation, inversion, and salt tectonics on a passive margin: Evolution of the Inner Kwanza Basin, Angola: Geological Society of America Bulletin, v. 114, no. 10, p. 1222-1244.

Hudec, M. R., and Jackson, M. P. A., 2004, Regional restoration across the Kwanza Basin, Angola: Salt tectonics triggered by repeated uplift of a metastable passive margin: AAPG Bulletin, v. 88, no. 7, p. 971-990.

Jackson, C. A. L., Jackson, M. P. A., and Hudec, M. R., 2015, Understanding the kinematics of salt-bearing passive margins: A critical test of competing hypotheses for the origin of the Albian Gap, Santos Basin, offshore Brazil: Geological Society of America Bulletin, v. 127, no. 11-12, p. 1730-1751.

Jackson, M. P. A., and Hudec, M. R., 2005, Stratigraphic record of translation down ramps in a passive-margin salt detachment: Journal of Structural Geology, v. 27, no. 5, p. 889-911.

Jackson, M. P. A., and Hudec, M. R., 2009, Interplay of Basement Tectonics, Salt Tectonics, and Sedimentation in the Kwanza Basin, Angola, AAPG: Cape Town, South Africa.

Jackson, M. P. A., and Hudec, M. R., 2017, Salt Tectonics: Principles and Practice, Cambridge, Cambridge University Press.

Jackson, M. P. A., Hudec, M. R., Jennette, D. C., and Kilby, R. E., 2008, Evolution of the Cretaceous Astrid thrust belt in the ultradeep-water Lower Congo Basin, Gabon: AAPG Bulletin, v. 92, no. 4, p. 487-511.

Karner, G. D., and Driscoll, N. W., 1999, Tectonic and stratigraphic development of the West African and eastern Brazilian Margins: insights from quantitative basin modelling: Geological Society, London, Special Publications, v. 153, no. 1, p. 11-40.

Karner, G. D., Driscoll, N. W., and Barker, D. H. N., 2003, Syn-rift regional subsidence across the West African continental margin: the role of lower plate ductile extension: Geological Society, London, Special Publications, v. 207, no. 1, p. 105-129.

Lundin, E. R., 1992, Thin-skinned extensional tectonics on a salt detachment, northern Kwanza Basin, Angola: Marine and Petroleum Geology, v. 9, no. 4, p. 405-411.

Marton, L. G., Tari, G. C., and Lehmann, C. T., 2000, Evolution of the Angolan passive margin, West Africa, with emphasis on post-salt structural styles: Atlantic Rifts and Continental Margins, v. 115, p. 129-149.

Moulin, M., Aslanian, D., Olivet, J.-L., Contrucci, I., Matias, L., Géli, L., Klingelhoefer, F., Nouzé, H., Réhault, J.-P., and Unternehr, P., 2005, Geological constraints on the evolution of the Angolan margin based on reflection and refraction seismic data (ZaïAngo project): Geophysical Journal International, v. 162, no. 3, p. 793-810.

Peel, F. J., 2014, The engines of gravity-driven movement on passive margins: Quantifying the relative contribution of spreading vs. gravity sliding mechanisms: Tectonophysics, v. 633, p. 126-142.

Pichel, L. M., Jackson, C. A. L., Peel, F., and Dooley, T. P., 2019, Base-salt relief controls salt-tectonic structural style, São Paulo Plateau, Santos Basin, Brazil: Basin Research, v. 32, no. 3, p. 453-484.

Pichel, L. M., Peel, F., Jackson, C. A. L., and Huuse, M., 2018, Geometry and kinematics of salt-detached ramp syncline basins: Journal of Structural Geology, v. 115, p. 208-230.

Quirk, D. G., Schødt, N., Lassen, B., Ings, S. J., Hsu, D., Hirsch, K. K., and Von Nicolai, C., 2012, Salt tectonics on passive margins: examples from Santos, Campos and Kwanza basins: Geological Society, London, Special Publications, v. 363, no. 1, p. 207-244.

Rowan, M., Peel, F., and Vendeville, B., 2004, Gravity-driven Fold Belts on Passive Margins, *in* McClay, K. R., ed., Thrust Tectonics and Hydrocarbon Systems, Volume 82, AAPG Memoir, p. 157-182.

Rowan, M. G., Jackson, M. P. A., and Trudgill, B. D., 1999, Salt-Related Fault Families and Fault Welds in the Northern Gulf of Mexico: AAPG Bulletin, v. 83, no. 9, p. 1454-1484.

Rowan, M. G., and Ratliff, R. A., 2012, Cross-section restoration of salt-related deformation: Best practices and potential pitfalls: Journal of Structural Geology, v. 41, p. 24-37.

Serié, C., Huuse, M., Schødt, N. H., Brooks, J. M., and Williams, A., 2017, Subsurface fluid flow in the deep-water Kwanza Basin, offshore Angola: Basin Research, v. 29, no. 2, p. 149-179.

Valle, P. J., Gjelberg, J. G., and Helland-Hansen, W., 2001, Tectonostratigraphic development in the eastern Lower Congo Basin, offshore Angola, West Africa: Marine and Petroleum Geology, v. 18, no. 8, p. 909-927.

Vendeville, B. C., and Jackson, M. P. A., 1992a, The fall of diapirs during thin-skinned extension: Marine and Petroleum Geology, v. 9, no. 4, p. 354-371.

Vendeville, B. C., and Jackson, M. P. A., 1992b, The rise of diapirs during thin-skinned extension: Marine and Petroleum Geology, v. 9, no. 4, p. 331-354.

Vendeville, B. C., and Nilsen, K. T., Episodic Growth of Salt Diapirs Driven By Horizontal Shortening, *in* Proceedings Gulf Coast Section SEPM Foundation 16th annual research conference, Houston, Texas, 1995, p. 285-295.

Von Nicolai, C., 2011, The Interplay of Salt Movements and Regional Tectonics at the Passive Continental Margin of the South Atlantic, Kwanza Basin [Unpublished PhD thesis]: Universität Potsdam.

Wagner, B. H., and Jackson, M. P. A., 2011, Viscous flow during salt welding: Tectonophysics, v. 510, no. 3-4, p. 309-326.

Tables Captions

Table 1: Compilation of previously published ages for key seismic reflections identified in the Outer Kwanza Basin and comparison to seismic-stratigraphic framework defined in this study.

Table 2: Geometry and origin of key salt structures identified in the study area. Seismic data courtesy of CGG Multi-Client.

Table 3: Geometry and origin of key supra-salt structures identified in the study area. Seismic data courtesy of CGG Multi-Client.

Figures Captions

Figure 1: Schematic diagram illustrating the types of salt and overburden structures that form in response to the flow of salt across base-salt relief. Salt is thin (t) across the base-salt high block and thick (T) adjacent to this. (a) During the early stages of flow onto a landward-dipping ramp, convergent intrasalt streamlines drive an increase in salt flux, and an acceleration in salt and its overburden. Contraction and salt thickening occur, allowing salt velocity to increase through time as basal drag is minimized (see below). (b) In the presence of an overburden, salt anticlines, capped by salt-cored buckle folds, can form at the top of a landward-dipping ramp. Polyharmonic buckle folds, which decrease in wavelength upwards, may form due to syn-translation thickening of overburden. Similar geometries are observed and kinematics are inferred from our study area (Fig. 5b and c). (c) During the latter stages of salt flow across a landward-dipping base-salt ramp, extensional structures form (and may dissect earlier-formed contractional structures) across the crest of the high block due to an increase in salt velocity generated by an earlier phase of salt contraction and thickening. Further downdip, at the top of a seaward-dipping ramp, another flux mismatch occurs where thinner, slower-moving salt meets thicker, faster-moving salt; this generates a so-called ‘extensional hinge’. Further downdip, at the base of this ramp another salt flux mismatch occurs, with faster moving salt on the ramp meeting thicker, slowing moving salt in the adjacent low; this generates a so-called ‘contractional hinge’. Note the types of salt and overburden structures arising due to the interaction between flowing salt and base-salt relief (figures redrawn from Jackson and Hudec, 2017; Dooley et al., 2017; 2018).

Figure 2: a) Simplified regional structural map illustrating the key tectonic features and domains offshore Angola, (b) Regional geoseismic section across the Outer Kwanza Basin, offshore Angola. The approximate location of the study area is indicated by the red box. Note the

presence of prominent base-salt relief, related to the underlying (i.e. sub-salt), rift-related, horst-and-graben system (modified from Marton et al., 2000; Hudec and Jackson, 2002, 2004; Moulin et al., 2005; Jackson and Hudec, 2005; Guiraud et al., 2010; Serié et al., 2017; GEBCO Compilation Group, 2020).

Figure 3: Simplified regional tectonostratigraphic framework of the Outer Kwanza Basin, offshore Angola. Note the protracted, multiphase salt-tectonics that are associated with significant seaward (i.e. to the SW) flow and rotation of salt and its overburden (adapted from Hudec and Jackson, 20014; Evans and Jackson, 2019).

Figure 4: (a) Depth-structure map (left) and interpretative sketch map (right) of the base-salt seismic horizon. These maps illustrate significant base-salt relief associated with complex, landward- and seaward-dipping ramps (highlighted in red), the most north-eastern of which are associated with the Flamingo Platform. (b) Isochron map (left) and interpretative sketch map (right) of the Aptian salt layer, illustrating the morphology and distribution of salt structures and flanking (primary) welds (see Table 2 for detailed description of salt structure geometry and origin). (c) Depth-structure map (left) and interpretative sketch map (right) of the top Albian seismic horizon. This map illustrates the types and distributions of supra-salt (i.e. overburden) faults and folds (see Table 3 for description of each type of supra-salt faults).

Figure 5: Margin-parallel (i.e. normal to regional base-salt dip and bulk translation direction) seismic profiles illustrating salt-related structural styles (section location shown in Fig. 4). (a) NW-SE-to-NE-SW-trending cross-section showing the salt and overburden structures and their present spatial relationships to base-salt highs and lows. This seismic profile illustrates salt walls, salt-detached strike-slip faults, and outer-arc extension faults above turtle anticlines. (b) NW-SE-trending cross-section showing polyharmonic salt anticlines (SA1), broadly located above areas where the base-salt is relatively flat. (c) Zoom in of (b), highlighting the detailed geometry of and overburden seismic-stratigraphic architecture associated with polyharmonic salt anticlines located just downdip of a SE-dipping base-salt ramp. Note the presence of intra-Albian growth strata. (d) NW-SE-trending cross-section illustrating salt-detached strike-slip fault adjacent to a SE-dipping base-salt ramp, outer-arc bending-related normal faults above a squeezed salt anticline, and a relic horn at the crest of the (extensionally) collapsed salt wall. For more details on the geometry and origin of salt and overburden structures, see Tables 2 and 3, respectively. Seismic data courtesy of CGG Multi-Client.

Figure 6: Margin-perpendicular (i.e. parallel to regional base-salt dip and bulk translation direction) seismic profiles illustrating the styles of salt-related contractional structures observed in the northern part of the study area (section location shown in Fig. 4). (a) NE-SW-trending cross-section showing salt anticlines (SA4-6) that may (i.e. central and right-hand anticlines) be capped by salt-detached normal and thrust faults. These anticlines are developed at the base (i.e. south-westwards) of a major seaward-dipping ramp. (b) NE-SW-trending cross-section illustrating salt anticlines (SA1-3) and complex salt walls; the latter is overlain by a basinward-dipping monocline and several ramp syncline basins (RSBs). (c) NE-SW-trending cross-section illustrating outer-arc bending-related normal faults capping a squeezed salt anticline (SN1). Further to the northeast, a squeezed salt wall (SS1) is located at the base of the seaward-dipping ramp and is itself capped by several RSBs. The RSBs record seaward translation of salt and its overburden (see text). Seismic data courtesy of CGG Multi-Client.

Figure 7: Margin-perpendicular (i.e. parallel to regional base-salt dip and bulk translation direction) seismic profiles illustrating the styles of salt-related contractional structures observed in the central and southern part of the study area (section location shown in Fig 4). (a) NE-SW cross-section showing diapir fall above complex salt wall (SW2) in the centre, while the complex salt walls (SS2-3) with associated NE and SW-dipping thrust faults developed above downdip of the NW-trending, SW-dipping ramp. (b) NE-SW cross-section showing polyharmonic, salt anticline (SA1) in the south west, while in the centre the complex salt wall (SW2) are presented. Further northeast, RSBs are developed above downdip, seaward-dipping of Flamingo platform. (c) NE-SW cross-section showing the complex salt wall (SW2) in the centre above downdip, seaward-dipping of local structural high. Seismic data courtesy of CGG Multi-Client.

Figure 8: (a) A composite map illustrating the present spatial relationship between structures present at the base-of-salt (taken from Fig. 4a) and overlying salt structures (taken from Fig. 4b). (b) A composite map illustrating the present spatial relationship between structures at the base-of-salt (taken from Fig. 4a) and overlying, supra-salt structures defined at the top Albian structural level (taken from Fig. 4c).

Figure 9: Structural restoration of margin-perpendicular (i.e. parallel to regional base-salt dip and bulk translation direction) seismic profiles (Figs 6a and 7a, c) illustrating the evolution of various salt and overburden structures in the Outer Kwanza Basin (see Appendix C for a larger version of the figures). (a) Restoration of a NW-SE-trending seismic profile in the south of the study area, crossing structural-high Y; (b) Restoration of a NW-SE-trending seismic profile in the

centre of the study area, crossing structural-high W; (c) Restoration of a NW-SE-trending seismic profile in the north of the study area, crossing structural-high V (see Appendix A for detailed documentation of the key methods and assumptions).

Figure 10: Graph showing the cumulative horizontal translation of salt an overburden in each of the cross-sections shown in Figure 9. The cumulative translation (i.e. the left vertical scale) are recorded in each absolute time (i.e. horizontal scale) from the seismic stratigraphic horizon. These cumulative translations are compared with the cumulative translation (i.e. the left vertical scale) and rotation (i.e. the right vertical scale) of Evan and Jackson (2019).

Figure 11: Map-view schematic restorations of salt and overburden structures from (a) the Late Albian to (g) Present; this is based on time-constrained horizontal translation magnitudes presented in the structural restorations shown in Figures 9 and 10, and information on RSB-constrained, salt and overburden rotations presented by Evans and Jackson (2019) (see text for full description).

Figure 12: Physical model investigating the effects of a local sub-salt high block (SSH) on the down-dip (i.e. to-the-right) flow of salt, illustrating the range of salt and overburden structures that can form (from Dooley et al., 2018). This situation is similar to that observed on many salt-bearing passive margins, including the Outer Kwanza Basin, offshore Angola (i.e. compare with the sub-salt high blocks V-Z observed in Fig. 4a). (a) Overhead photographs of the models at various time steps (i-iv) showing the variable distribution and overprinting of extensional and contractional salt and overburden structures, and rotation of salt and overburden structures at the up-dip (up to 36^{o}) and down-dip (up to 67^{o}) edge of the SSHs; and (b) the local base-salt high act as salt flow perturbation, resulting in salt flow channelization (i.e. convergent and divergent flow). For full details of the model design and set-up, please see Dooley et al. (2018).

Table

Table 1

Age	Horizon		
	This study	Previous publication	
Late Miocene	Top of Miocene	Top of Miocene	Hudec and Jackson (2004)
		Mi	Serie et al (2015)
Middle Miocene	M2		
Early Miocene	M1		
Oligocene	Oligocene	Og	Serie et al (2015)
		Top Oligocene	Hudec and Jackson (2004)
		O2	Valle et al (2001)
Eocene	Eocene	Eo	Serie et al (2015)
		E1	Valle et al (2001)
Albian	Albian	Alb	Serie et al (2015)
Late Aptian	Salt		
Middle Aptian	Base salt		

Table 2

Map and text name	Example	Geometries: Diagnostic description	Geometries: Ramp trend association	Geometries: Dimension Length (km)	Geometries: Dimension Width (km)	Geometries: Dimension Height	Geometries: Fault association	Genetic Interpretation: Driving Forces Initiation	Genetic Interpretation: Driving Forces Evolution	Genetic Interpretation: Salt-related deformations Initiation	Genetic Interpretation: Salt-related deformations Evolution
Salt anticline (SA)	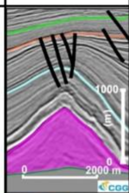 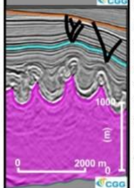	◦Low amplitude, long wavelengths of rounded salt upwellings ◦Locally polyharmonic, high amplitude, short wavelength of rounded salt upwellings ◦Concordant contact with overburden ◦It is laterally merged into salt walls or intersected by strike slip faults	Trend broadly parallel to NW- or N-trending ramps; located above upper tip of either landward-or basinward-dipping ramps Trend oblique to NW-trending and parallel to N-trending ramps; broadly located above relatively flat relief	at least 1.3	at least 0.5	Up to 0.7	◦NW-trending symmetric outer-arc extensional faults locally cut-off the roof ◦NW, N-trending, landward-dipping thrust faults are locally above the crest, or NW, N-trending, basinward-dipping salt-detached normal faults cut off the fold limb	Local contraction due to retardation of salt flow above base-salt high block Local contraction, due to retardation of salt flow, whilst overburden thicken above base-salt high block	Local extensions are located: (i) at the upper tip of basinward -dipping ramps due to difference in salt flux (ii) above base-salt high blocks due to increasing of salt velocity flow	Salt anticlines, with or without thrust faults	Reactive salt walls, salt anticlines dissected by salt-detached normal faults
Squeezed salt anticline (SN)	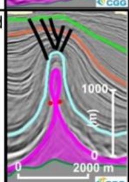	◦Triangular salt pedestals with a secondary salt weld and a bulb-shaped head ◦ It is laterally intersected by strike-slip faults	Trend parallel to NW-trending ramps; located above upper-tip of basinward-dipping ramps	1.8 - 6	Up to 3 on salt pedestal	Up to 1.1	NW-trending symmetric outer-arc extensional faults cutoff the roof	Local contraction due to due to retardation of salt flow above base-salt high block	Local contraction due to salt flow encounter slower-moving salt at the base of base-salt high block	Salt anticlines	Squeezed salt anticlines
Salt wall (SW)	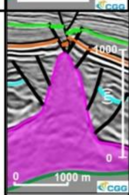 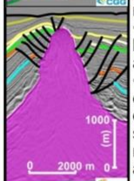	◦Symmetric triangular profiles ◦The diapir crest are geometrically pointed (i.e. reactive piercement) or rounded while the roof is arched above it (i.e. active piercement) ◦A relic horn is locally observed above the crest ◦It is laterally changed into different types of salt wall (i.e. reactive and active salt wall)	Trend broadly parallel to NW, N and NE-trending, with locally oblique to NW-trending ramps; located broadly above either downdip of or at the base of basinward-dipping ramps, or locally above relatively flat relief	Up to 47	1.1 - 4.27	Up to 3	NW, N, NE-trending, inward-dipping, locally rotated, salt-detached normal faults cutoff the flank and/or are over the crest	Local extension: (1) above base-salt high blocks due to salt velocity increment (2) above the upper tip of-basinward-dipping ramps due to salt flux mismatch (i.e. low to high)	Local extension due to salt flow to another part of salt wall Local contraction due to salt flow encounter slower-moving salt at the base of ramps	Reactive salt wall	Diapir fall Active piercement (Active rise)
Squeezed or thrusted roof salt wall (SS)	 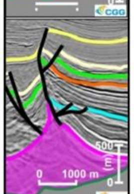	◦A triangular salt pedestal, a local secondary salt weld and a local bulb-shaped head ◦It is laterally intersected by strike-slip faults	Parallel to NW -trending ramps; broadly located at the base of basinward-dipping ramps and locally located above relatively flat relief	Up to 5	Up to 2 on salt pedestal	Up to 1.9	◦NW, N, NE-trending, inward-dipping, salt-detached normal faults cutoff the flank and/or the triangular pedestal ◦NW-trending, basinward, landward-dipping thrust fault are locally over the crest ◦ Outer arc-extensional faults are over the roof	Local extension: (1) above base-salt high blocks due to salt velocity increment; (2) above the upper tip of basinward-dipping ramps due to salt flux mismatch (i.e. low to high)	◦Local contraction due to salt flow encounter slower-moving salt at the base of base-salt high block ◦Local contraction due to salt flow encountering salt weld, which acts as a buttress	Reactive salt wall	Squeezed or thrusted roof salt wall
Salt roller (SR)	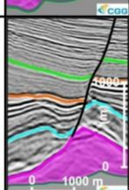	◦A low amplitude, asymmetric triangular profile comprises of a gently and a steeply dipping flank ◦It is laterally intersected by strike-slip faults	Parallel to NW -trending ramps; broadly located above downdip of basinward-dipping ramps	Up to 1.6	Up to 0.4	Up to 0.2	◦NW, N, NE-trending, inward-dipping, salt-detached normal faults cutoff a more steeply dipping flank	Local extension: (1) above base-salt high blocks due to salt velocity increment; (2) above the upper tip of basinward-dipping ramps due to salt flux mismatch (i.e. low to high)		Salt roller	

Legend: Seabed; Top Late Miocene; Top Middle Miocene; Top Early Miocene; Top Oligocene; Top Eocene; Top Albian; Top Salt; Base Salt; • Primary Weld

Table 3

Map and text name	Example	Geometries: Diagnostic description	Geometries: Orientation: Dip direction	Geometries: Orientation: Ramp trend association	Geometries: Dimension: Length (km)	Geometries: Dimension: Dip (o)	Geometries: Max. throw (m)	Offset	Stratigraphic Association	Genetic
Salt-detached normal fault	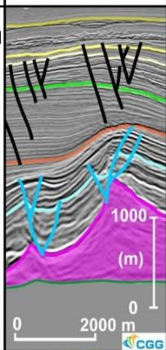	◦Planar and/or locally rotated normal or listric growth faults that sole into salt layer ◦In map view, the fault arrays form arcuate-to-planar patterns, which laterally die out into salt structures	Locally inward-dipping Toward salt walls; dominantly basinward and landward	Strike broadly parallel to NW, N, NE-trending, and, locally, oblique to NW-trending ramps; located either above relatively flat reliefs or downdip of basinward-dipping ramps	at least 2.5	56 - 86	up to 500	◦Normal offset at Albian-Eocene strata and, locally, at Albian-Holocene; lower fault tip dies out into the salt layer, and upper fault tip dies out into overburden	◦Generally, Eocene strata thicken toward the fault plane ◦ Locally, between isolated structural highs and the Flamingo platform, Albian or Oligocene-Holocene strata thicken toward the fault plane ◦ Locally, where active rise is observed, Oligocene and Middle Miocene strata thicken toward the fault plane ◦Locally, where the diapir fall is observed, Early and Late Miocene strata thicken toward the fault plane	◦Above base-salt high block, local extension due to salt velocity increment ◦ Above basinward-dipping ramp, local extension due to salt flux mismatch (i.e. low to high).
Outer-arc extensional fault	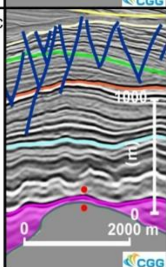	◦Planar normal faults form symmetric-to-asymmetric grabens, which are developed either on the hanging zone of an anticline or axial trace of a monocline ◦In map view, the fault array forms curved-to-planar patterns that are parallel to the underlying fold	Inward-dipping toward fold hinge zone; locally antithetic to salt-detached normal fault	Strike broadly parallel to underlying NW-or NE-trending ramps; located above relatively flat reliefs, a local structural high or downdip of basinward-dipping ramps	at least 2.0	70	up to 100	◦Planar normal offset between Albian and Middle Miocene strata depend on association of salt-related structures; both upper and lower fault tip die out into overburden	◦ Lack associated growth strata toward the fault plane	◦Outer arc bending due to folded strata related to: (i) extension associated with bending of rollover monocline, located on the hanging wall of salt detached normal fault; (ii) contraction of salt anticlines
Strike-slip fault	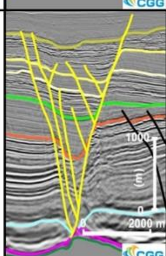	◦Planar normal growth faults that, locally form negative flower structures, and, locally, has partial coupling with base-salt ◦In map view, it forms linear patterns and piercing point on salt structures, salt-detached normal faults and thrust faults	South-east and north-west	Strike parallel to NE-trending ramps; located above relatively flat reliefs, or downdip of SE-, NW-dipping ramps	at least 10	62 - 87	up to 800 on dip slip; up to 3000 on strike	◦Normal offset from Albian to Eocene and, locally, to Holocene strata; lower fault tip dies out into salt layer and upper fault tip dies out into overburden	◦ Albian strata broadly tabular toward the fault plane ◦ Locally, Eocene-Oligocene strata, and Late Miocene-Holocene strata thicken toward the fault plane	◦Different translation rates due to different salt thickness and might be associated with base-salt relief oriented parallel to salt flow
Thrust fault	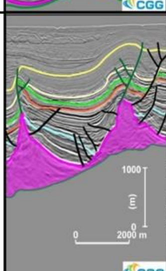	◦Planar thrust faults that sole into the crest of salt structures. ◦Antithetic extensional faults, an inverted wedge and growth folds are locally presented in the hanging wall of the fault ◦In map view, the fault forms planar-to-arcuate patterns, which laterally either merges into salt-detached normal fault or dies out into salt walls	Landward	Strike parallel to NW- or N-trending ramps; located above downdip of landward-dipping ramps	at least 10	45 - 70	up to 100	◦Reverse offset at Albian strata lower fault tip dies out into the crest of salt anticlines and upper fault tip dies out into Eocene strata	◦ Intra-Oligocene strata onlap onto growth folds that are associated with the thrust fault	◦Local contraction due to retardation of salt flow above base-salt high block
				Strike parallel to NW-trending ramps; located above downdip of basinward-dipping ramps			up to 500	◦Locally, reverse offset at Eocene-Middle Miocene strata; lower fault tip dies out into the crest of salt walls, and upper fault tip dies out into Late Miocene strata	◦Eocene strata thicken toward the fault plane ◦Oligocene-Early Miocene strata broadly tabular toward fault planes ◦Inverted wedge on Middle Miocene strata ◦Intra-Late Miocene strata onlap onto hanging wall of the fault plane	◦Local contraction due to salt flow encounter a salt weld, which acts as a buttress
			Basinward				up to 200	◦Reverse offset at Eocene-Middle Miocene strata; lower fault tip dies out into the crest of salt walls, and upper fault tip dies out into Late Miocene strata	◦Locally, Eocene strata thicken toward the fault plane ◦Locally, Oligocene strata broadly tabular toward the fault plane ◦Locally, inverted wedge on Early Miocene-Holocene strata ◦Late Miocene strata onlap onto inverted wedge and is truncated by Holocene strata	◦Local contraction due to salt flow encounter slower-moving salt at the base of base-salt high block

Legend: Seabed; Top Late Miocene; Top Middle Miocene; Top Early Miocene; Top Oligocene; Top Eocene; Top Albian; Top Salt; Base Salt; • Primary Weld

Figures

Figure 1

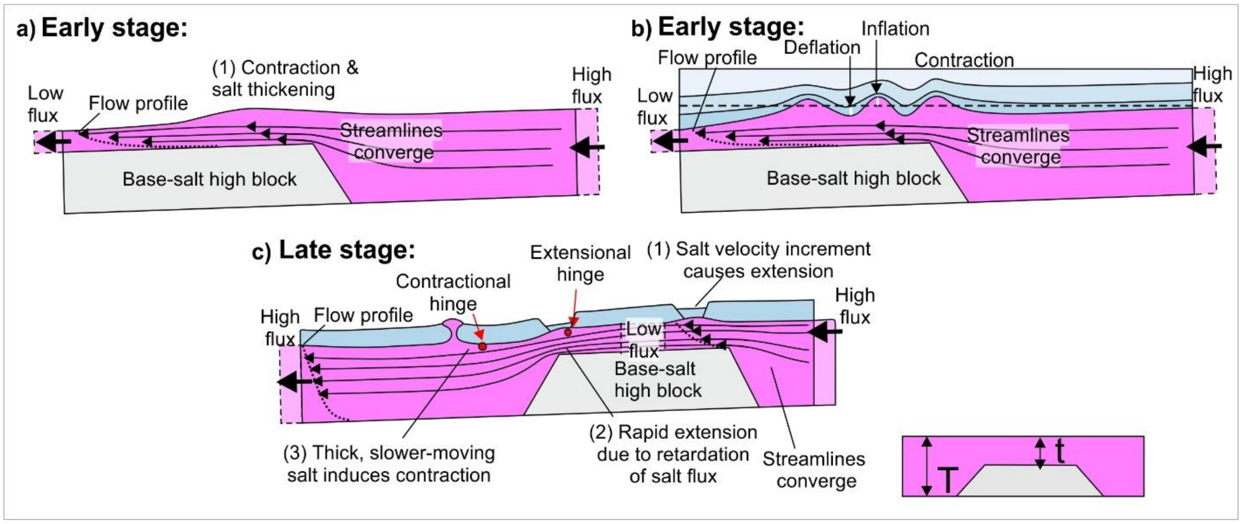

Figure 2

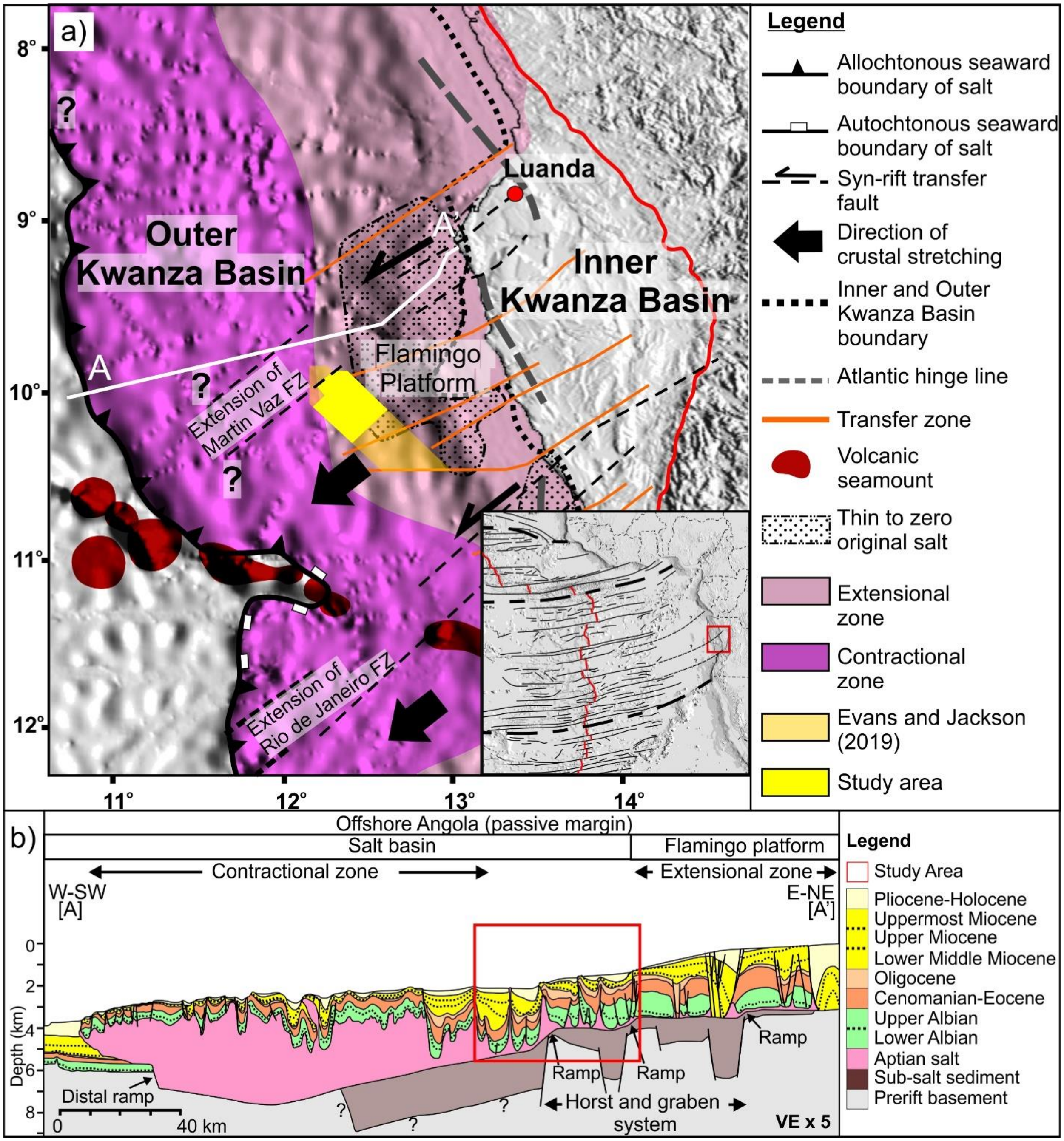

a)
8°
9°
10°
11°
12°
11°
12°
13°
14°
?
Outer Kwanza Basin
Inner Kwanza Basin
Luanda
A
A'
Flamingo Platform
Extension of Martin Vaz FZ
Extension of Rio de Janeiro FZ
Legend
Allochtonous seaward boundary of salt
Autochtonous seaward boundary of salt
Syn-rift transfer fault
Direction of crustal stretching
Inner and Outer Kwanza Basin boundary
Atlantic hinge line
Transfer zone
Volcanic seamount
Thin to zero original salt
Extensional zone
Contractional zone
Evans and Jackson (2019)
Study area
b)
Offshore Angola (passive margin)
Salt basin
Flamingo platform
Contractional zone
Extensional zone
W-SW [A]
E-NE [A']
Depth (km)
0
2
4
6
8
Distal ramp
0
40 km
Ramp
Ramp
Ramp
Horst and graben system
VE x 5
Legend
Study Area
Pliocene-Holocene
Uppermost Miocene
Upper Miocene
Lower Middle Miocene
Oligocene
Cenomanian-Eocene
Upper Albian
Lower Albian
Aptian salt
Sub-salt sediment
Prerift basement

Figure 3

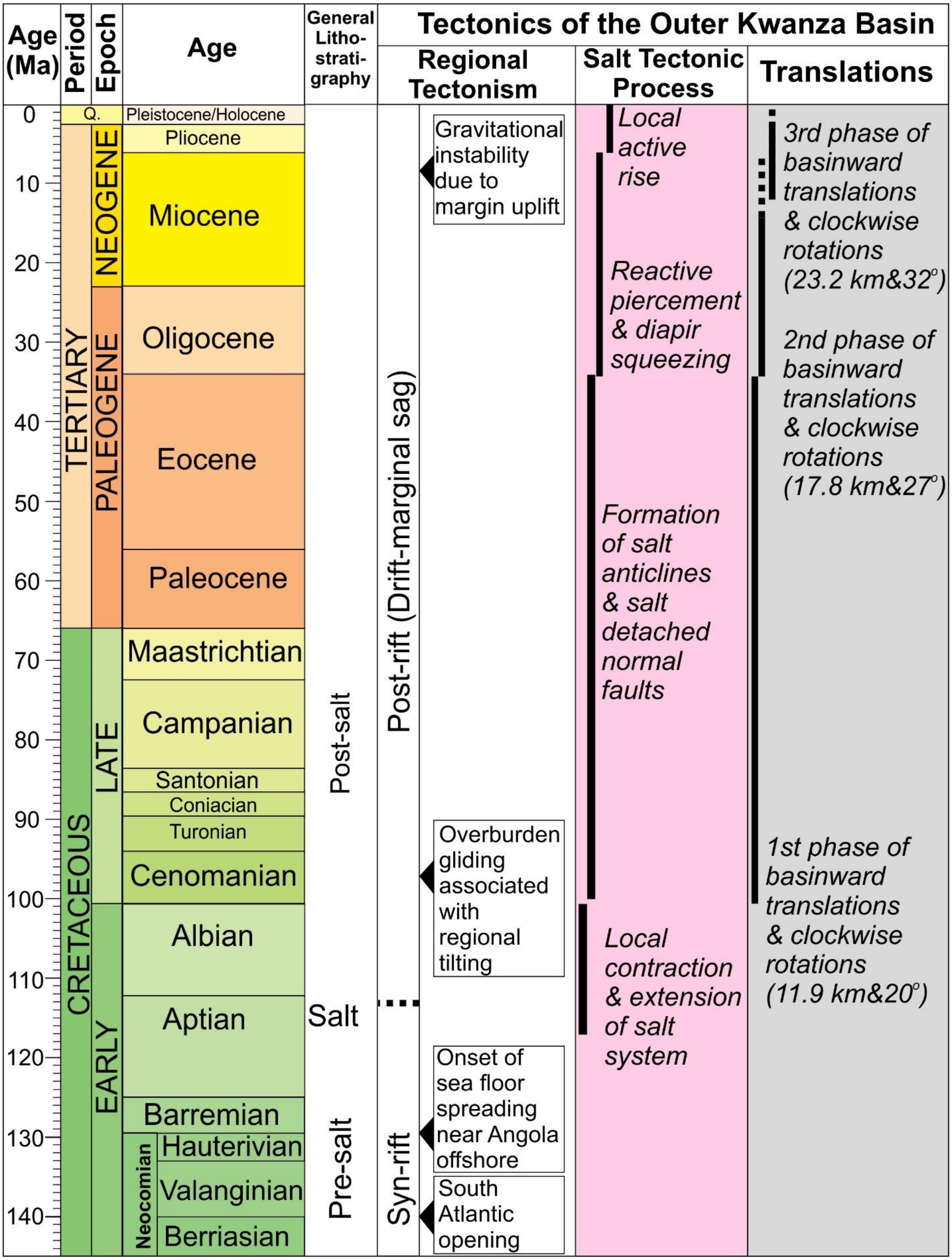
Age (Ma)
Period
Epoch
Age
General Litho-strati-graphy
Tectonics of the Outer Kwanza Basin
Regional Tectonism
Salt Tectonic Process
Translations
0
10
20
30
40
50
60
70
80
90
100
110
120
130
140
Q.
TERTIARY
CRETACEOUS
NEOGENE
PALEOGENE
LATE
EARLY
Neocomian
Pleistocene/Holocene
Pliocene
Miocene
Oligocene
Eocene
Paleocene
Maastrichtian
Campanian
Santonian
Coniacian
Turonian
Cenomanian
Albian
Aptian
Barremian
Hauterivian
Valanginian
Berriasian
Post-salt
Salt
Pre-salt
Post-rift (Drift-marginal sag)
Syn-rift
Gravitational instability due to margin uplift
Overburden gliding associated with regional tilting
Onset of sea floor spreading near Angola offshore
South Atlantic opening
Local active rise
Reactive piercement & diapir squeezing
Formation of salt anticlines & salt detached normal faults
Local contraction & extension of salt system
3rd phase of basinward translations & clockwise rotations (23.2 km&32°)
2nd phase of basinward translations & clockwise rotations (17.8 km&27°)
1st phase of basinward translations & clockwise rotations (11.9 km&20°)

931 Figure 4

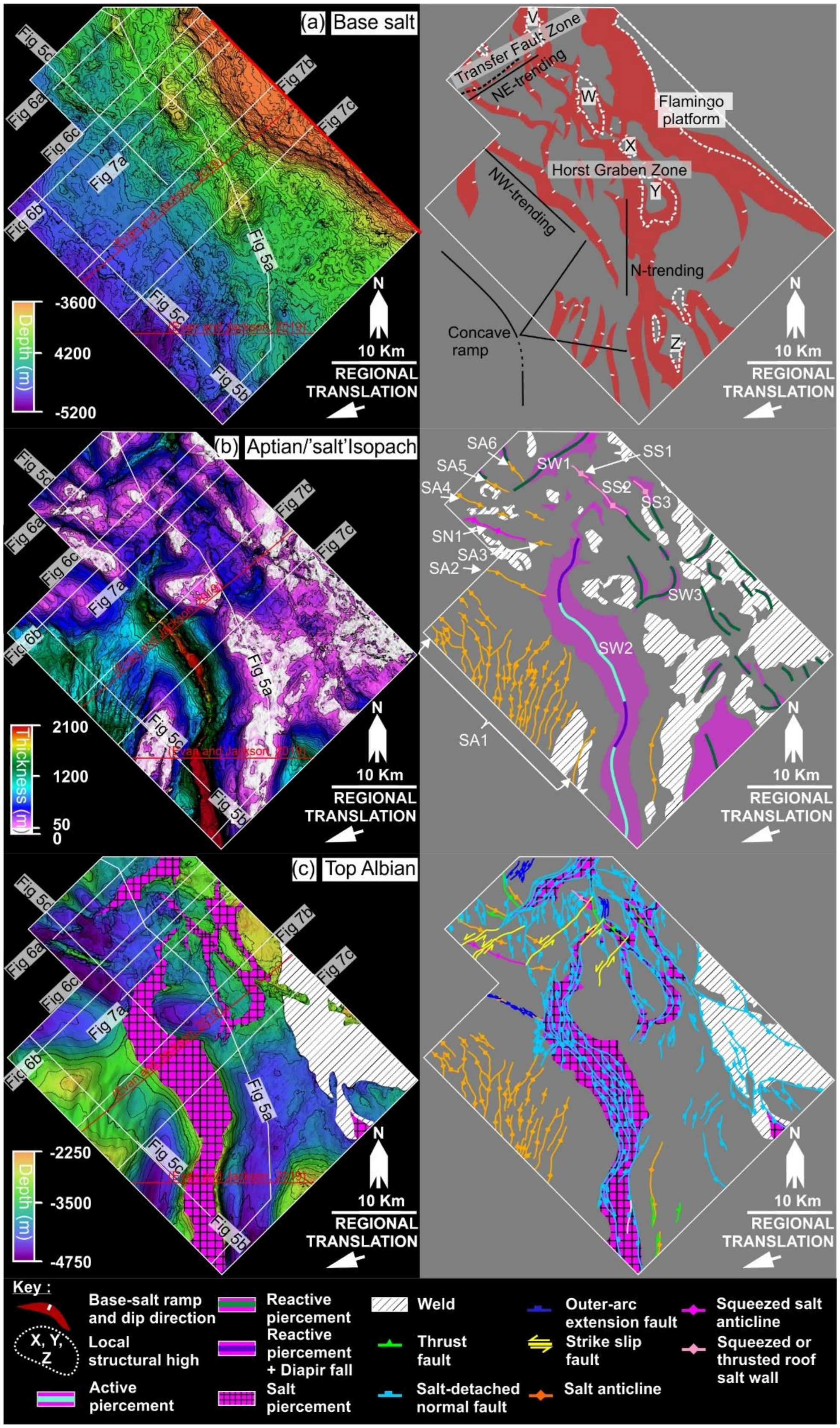

932

Figure 5

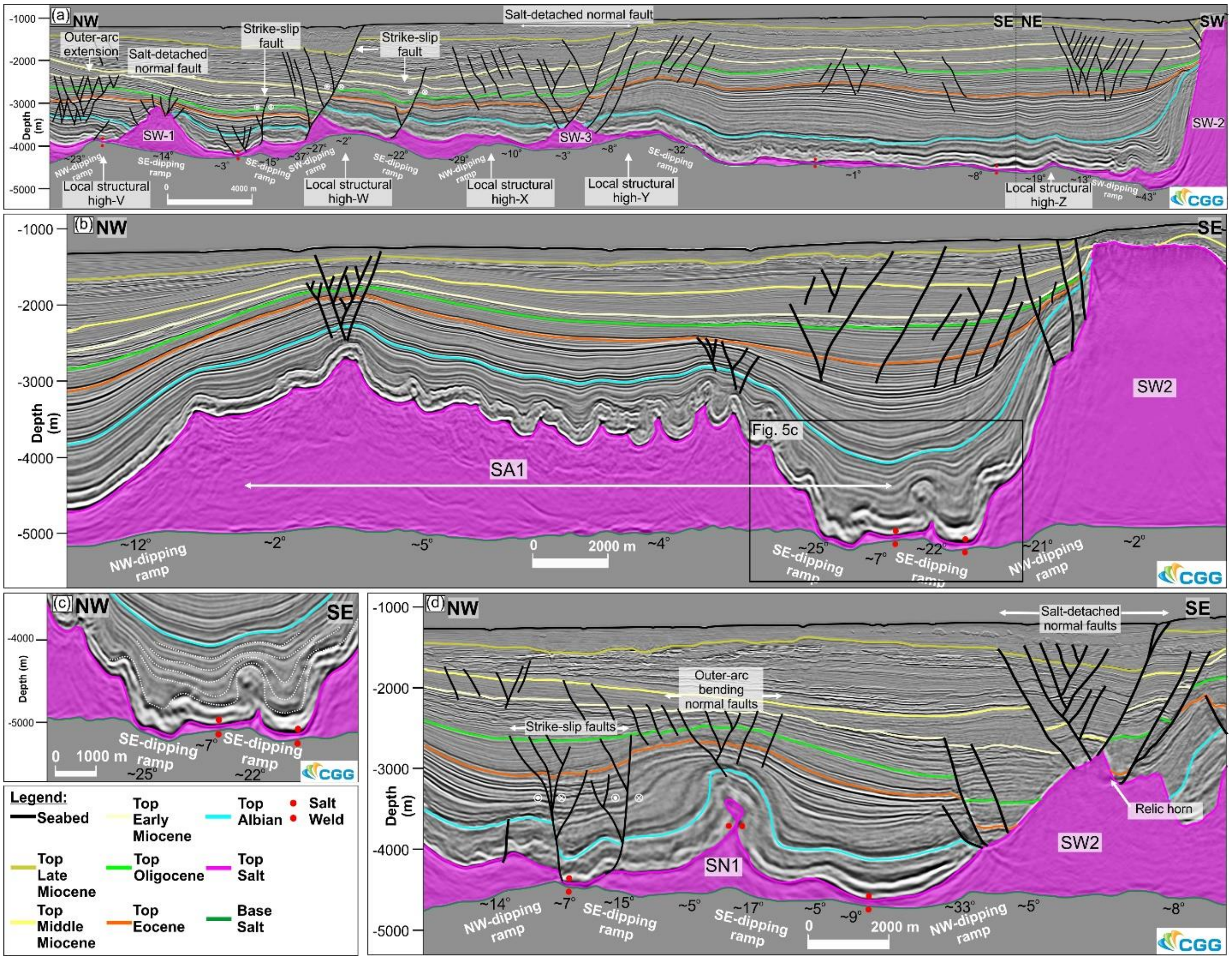
(a)
NW
SE
NE
SW
Salt-detached normal fault
Outer-arc extension
Salt-detached normal fault
Strike-slip fault
Strike-slip fault
SW-1
SW-3
SW-2
Depth (m)
Local structural high-V
Local structural high-W
Local structural high-X
Local structural high-Y
Local structural high-Z
NW-dipping ramp
SE-dipping ramp
SW-dipping ramp
4000 m
CGG
(b)
NW
SE
SA1
SW2
Fig. 5c
Depth (m)
~12°
NW-dipping ramp
~2°
~5°
2000 m
~4°
~25°
SE-dipping ramp
~7°
~22°
SE-dipping ramp
~21°
NW-dipping ramp
~2°
CGG
(c)
NW
SE
Depth (m)
1000 m
SE-dipping ramp
~7°
SE-dipping ramp
~25°
~22°
CGG
Legend:
Seabed
Top Early Miocene
Top Albian
Salt Weld
Top Late Miocene
Top Oligocene
Top Salt
Top Middle Miocene
Top Eocene
Base Salt
(d)
NW
SE
Salt-detached normal faults
Outer-arc bending normal faults
Strike-slip faults
Relic horn
SN1
SW2
Depth (m)
~14°
NW-dipping ramp
~7°
~15°
SE-dipping ramp
~5°
~17°
SE-dipping ramp
~5°
~9°
2000 m
~33°
NW-dipping ramp
~5°
~8°
CGG

948 Figure 6

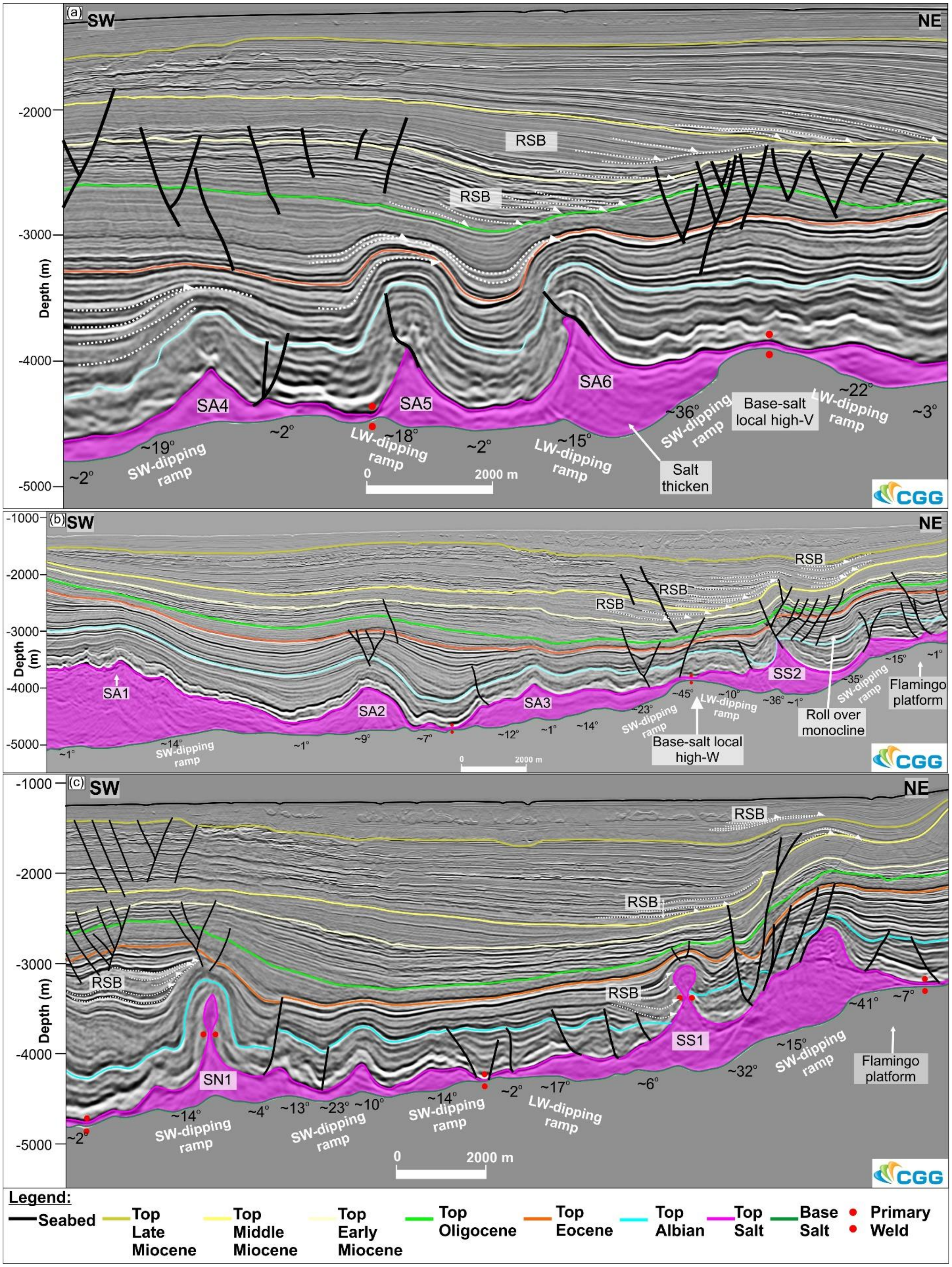

949

Figure 7

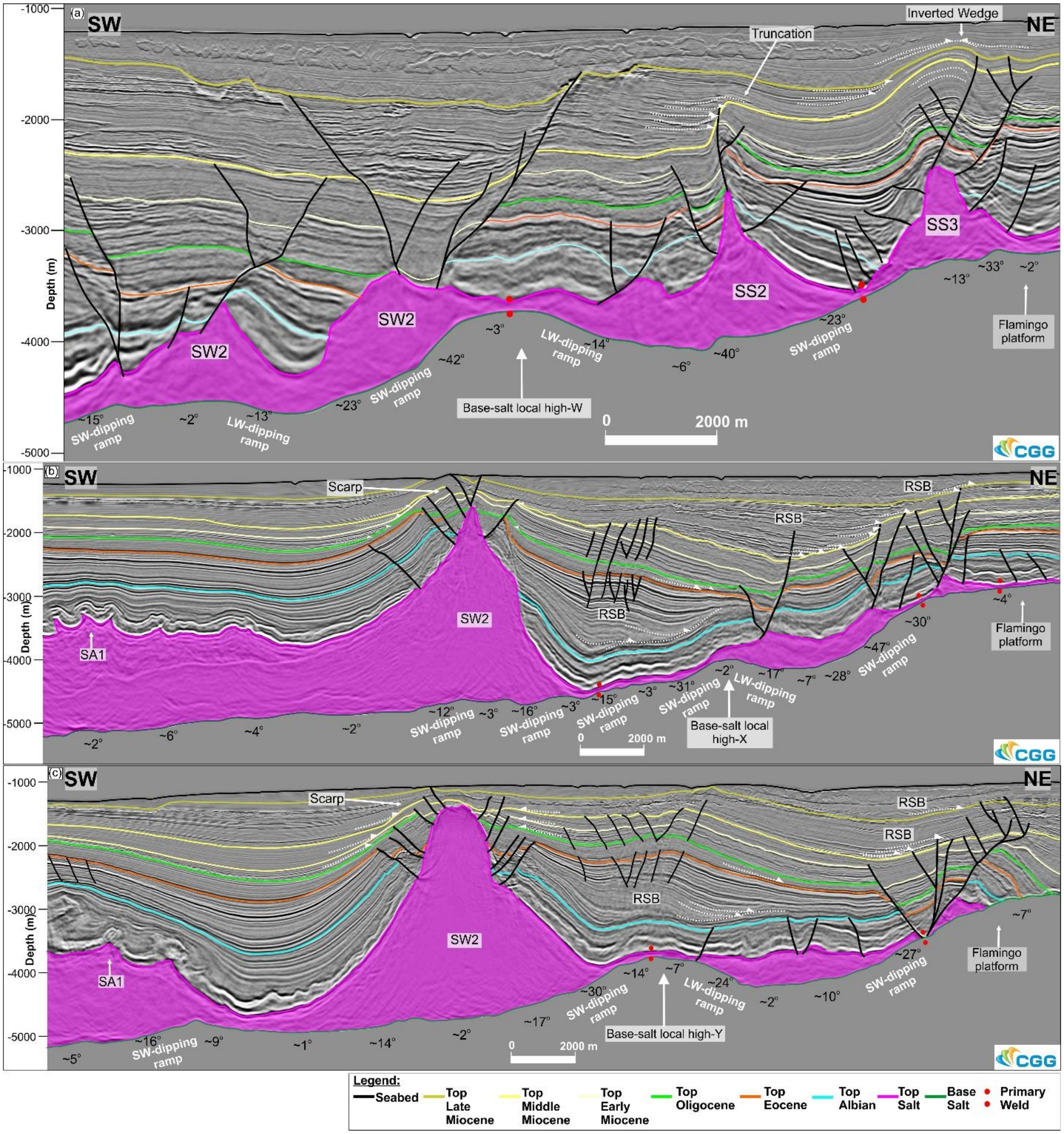

(a)
SW
NE
Inverted Wedge
Truncation
SW2
SW2
SS2
SS3
Depth (m)
SW-dipping ramp
LW-dipping ramp
Base-salt local high-W
Flamingo platform
0 2000 m
(b)
Scarp
RSB
SA1
Base-salt local high-X
(c)
Base-salt local high-Y
Legend:
Seabed
Top Late Miocene
Top Middle Miocene
Top Early Miocene
Top Oligocene
Top Eocene
Top Albian
Top Salt
Base Salt
Primary Weld

Figure 8

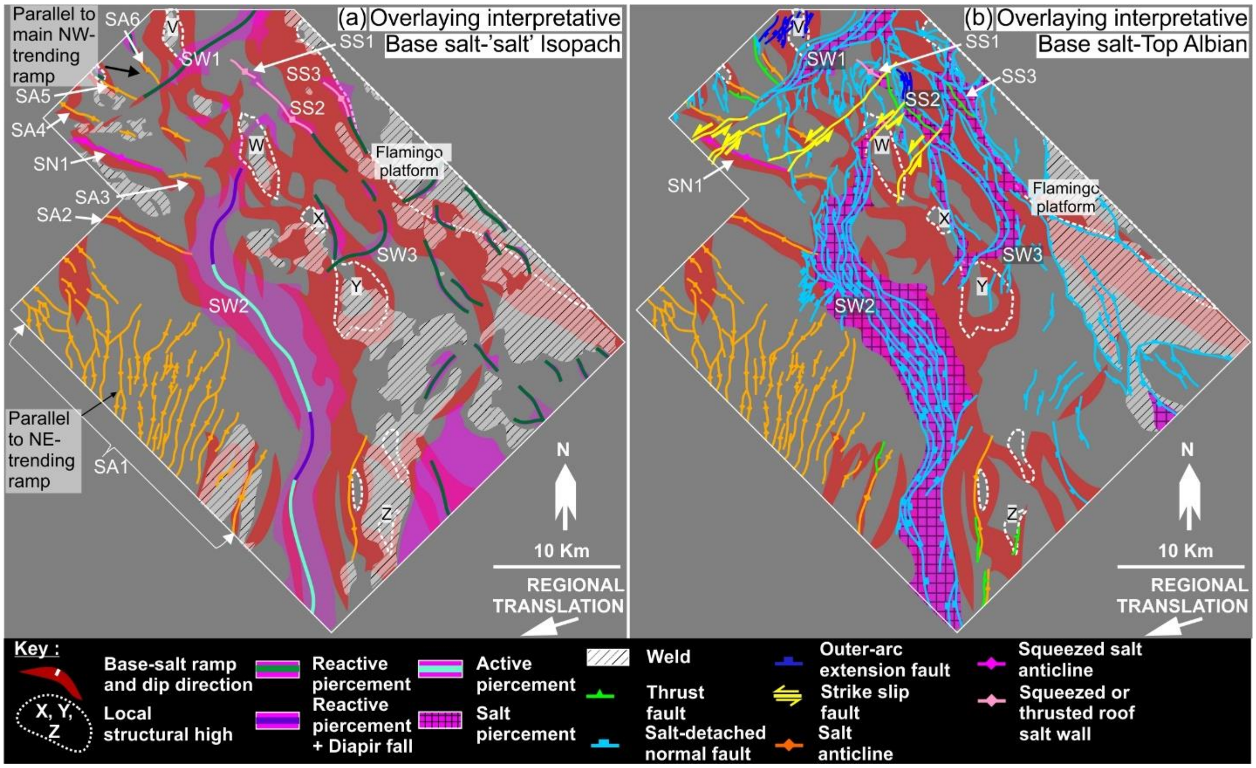
(a) Overlaying interpretative
Base salt-'salt' Isopach
Parallel to main NW-trending ramp
SA6
V
SW1
SS1
SS3
SS2
SA5
SA4
SN1
W
Flamingo platform
SA3
SA2
X
SW3
Y
SW2
Parallel to NE-trending ramp
SA1
Z
N
10 Km
REGIONAL TRANSLATION
(b) Overlaying interpretative
Base salt-Top Albian
V
SW1
SS1
SS2
SS3
W
SN1
Flamingo platform
X
SW3
Y
SW2
Z
N
10 Km
REGIONAL TRANSLATION
Key :
Base-salt ramp and dip direction
X, Y, Z
Local structural high
Reactive piercement
Reactive piercement + Diapir fall
Active piercement
Salt piercement
Weld
Thrust fault
Salt-detached normal fault
Outer-arc extension fault
Strike slip fault
Salt anticline
Squeezed salt anticline
Squeezed or thrusted roof salt wall

Figure 9

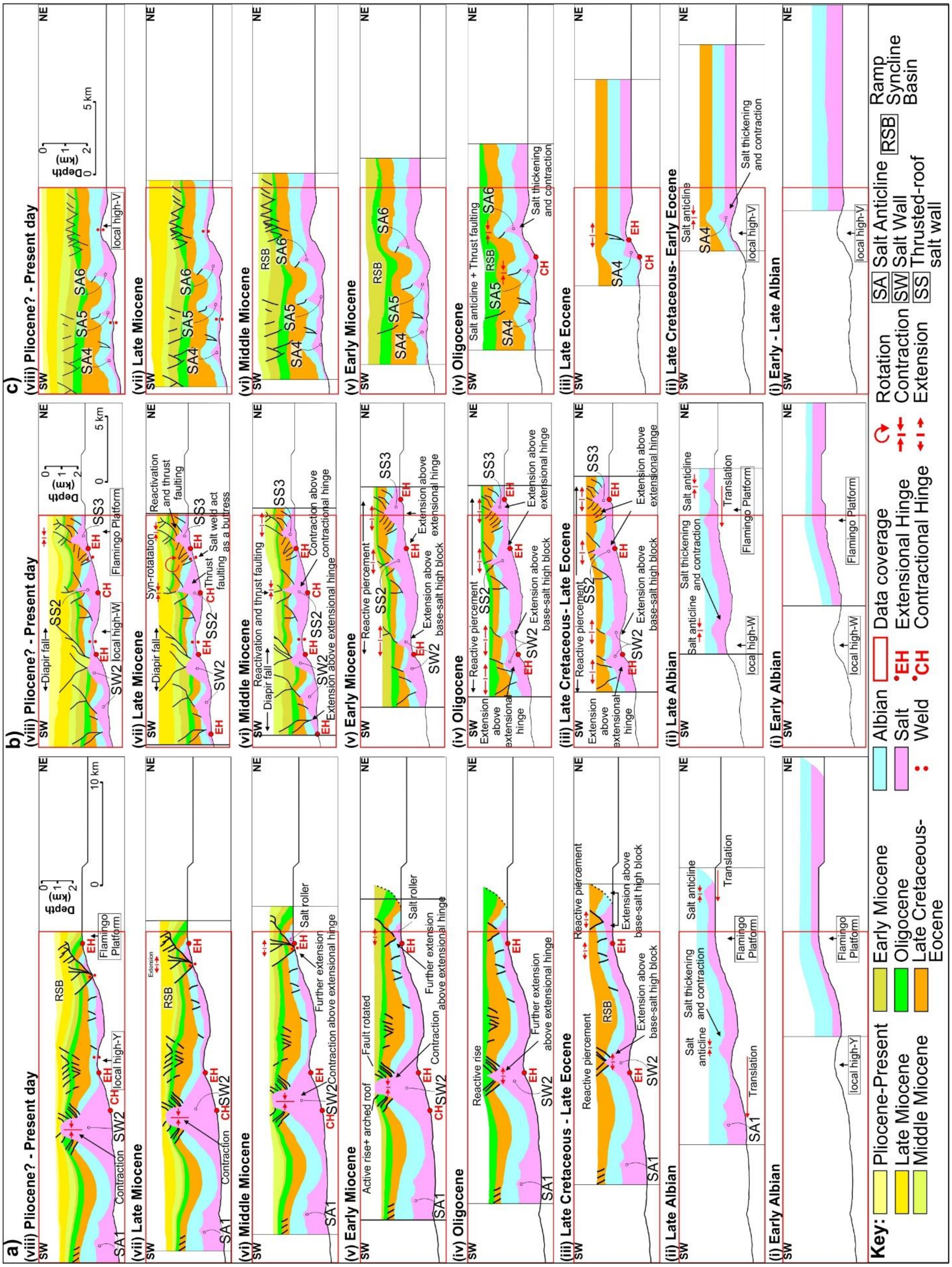

a)
b)
c)
(viii) Pliocene? - Present day
(vii) Late Miocene
(vi) Middle Miocene
(v) Early Miocene
(iv) Oligocene
(iii) Late Cretaceous - Late Eocene
(ii) Late Albian
(i) Early Albian
(iii) Late Eocene
(ii) Late Cretaceous- Early Eocene
(i) Early - Late Albian
SW
NE
Depth (km)
10 km
5 km
Flamingo Platform
local high-Y
local high-W
local high-V
Key:
Pliocene-Present
Late Miocene
Middle Miocene
Early Miocene
Oligocene
Late Cretaceous-Eocene
Albian
Salt
Weld
Data coverage
Extensional Hinge
Contractional Hinge
Rotation
Contraction
Extension
SA Salt Anticline
SW Salt Wall
SS Thrusted-roof salt wall
RSB Ramp Syncline Basin

Figure 10

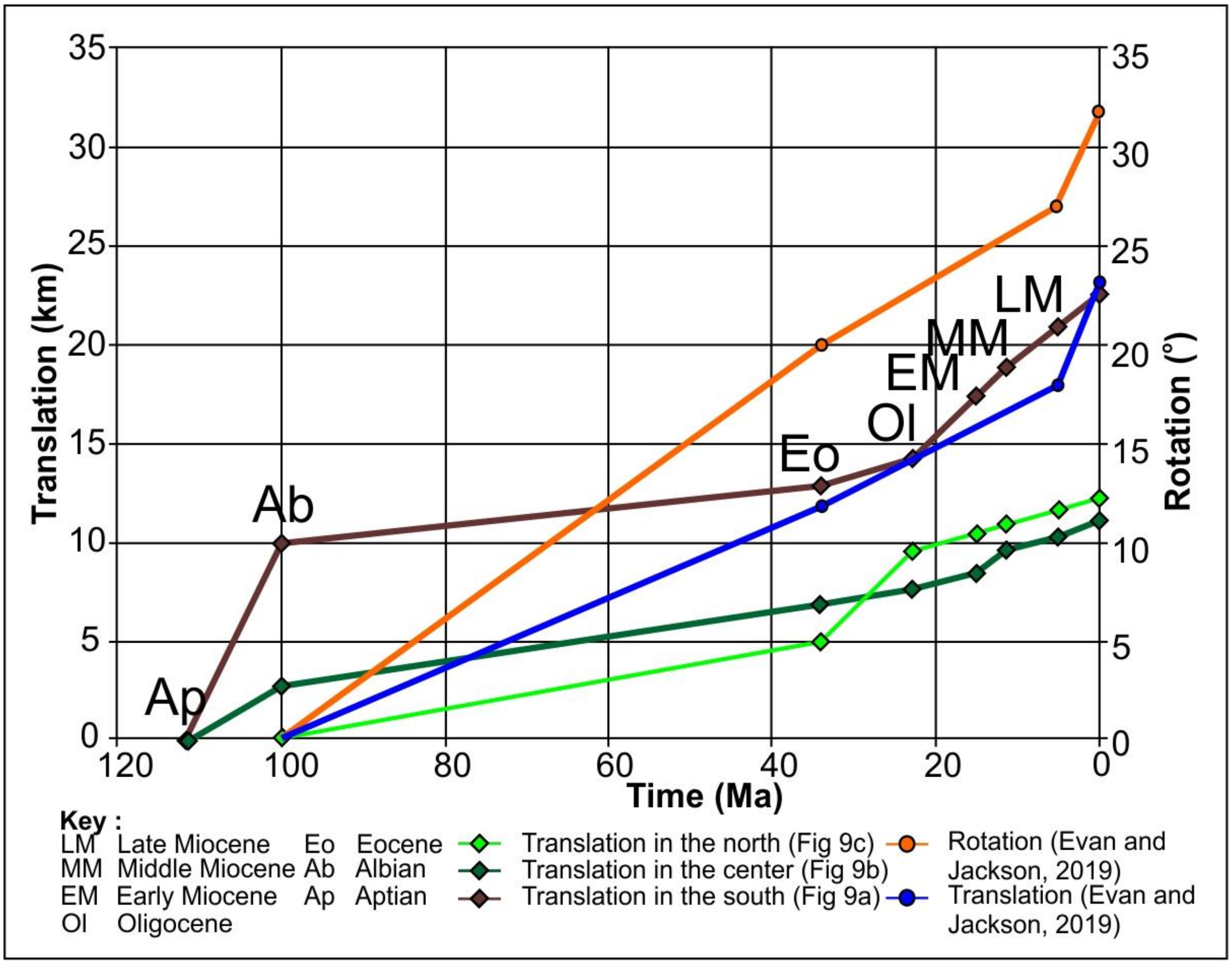
Translation (km)
Rotation (°)
Time (Ma)
Ap
Ab
Eo
Ol
EM
MM
LM
Key :
LM Late Miocene
MM Middle Miocene
EM Early Miocene
Ol Oligocene
Eo Eocene
Ab Albian
Ap Aptian
Translation in the north (Fig 9c)
Translation in the center (Fig 9b)
Translation in the south (Fig 9a)
Rotation (Evan and Jackson, 2019)
Translation (Evan and Jackson, 2019)

Figure 11

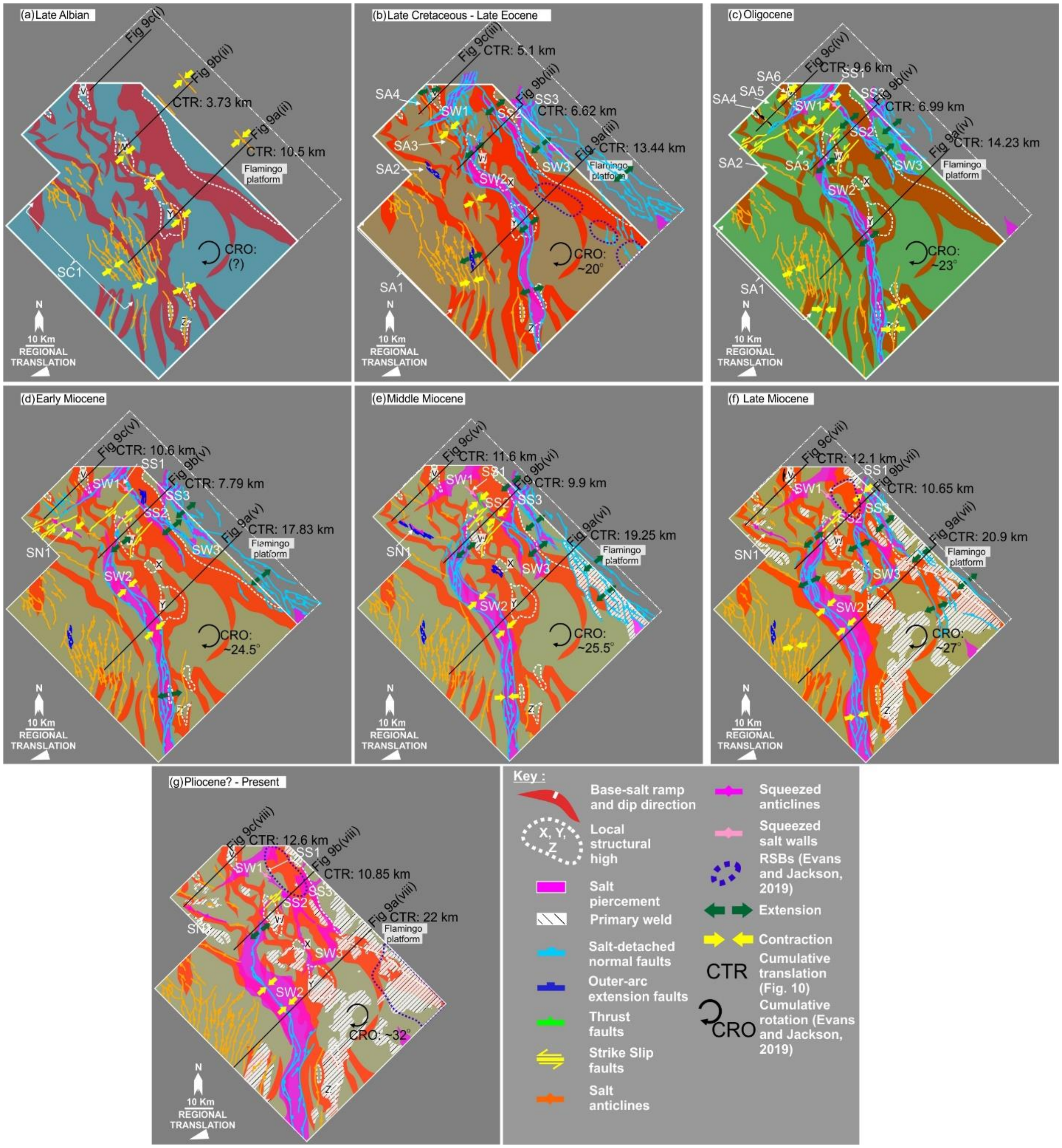

(a) Late Albian
CTR: 3.73 km
CTR: 10.5 km
Flamingo platform
CRO: (?)
SC1
(b) Late Cretaceous - Late Eocene
CTR: 5.1 km
CTR: 6.62 km
CTR: 13.44 km
CRO: ~20°
(c) Oligocene
CTR: 9.6 km
CTR: 6.99 km
CTR: 14.23 km
CRO: ~23°
(d) Early Miocene
CTR: 10.6 km
CTR: 7.79 km
CTR: 17.83 km
CRO: ~24.5°
(e) Middle Miocene
CTR: 11.6 km
CTR: 9.9 km
CTR: 19.25 km
CRO: ~25.5°
(f) Late Miocene
CTR: 12.1 km
CTR: 10.65 km
CTR: 20.9 km
CRO: ~27°
(g) Pliocene? - Present
CTR: 12.6 km
CTR: 10.85 km
CTR: 22 km
CRO: ~32°
10 Km
REGIONAL TRANSLATION
Key :
Base-salt ramp and dip direction
Local structural high
Salt piercement
Primary weld
Salt-detached normal faults
Outer-arc extension faults
Thrust faults
Strike Slip faults
Salt anticlines
Squeezed anticlines
Squeezed salt walls
RSBs (Evans and Jackson, 2019)
Extension
Contraction
CTR Cumulative translation (Fig. 10)
CRO Cumulative rotation (Evans and Jackson, 2019)

Figure 12: Physical model of Dooley et al (2018) (Not display, waiting for permission).